

Electronic Theses and Dissertations, 2020-

2022

Studies on Copper Indium based Oxide Transparent Semiconducting Thin Films.

Giji Skaria
University of Central Florida

 Part of the [Electrical and Computer Engineering Commons](#)
Find similar works at: <https://stars.library.ucf.edu/etd2020>
University of Central Florida Libraries <http://library.ucf.edu>

This Doctoral Dissertation (Open Access) is brought to you for free and open access by STARS. It has been accepted for inclusion in Electronic Theses and Dissertations, 2020- by an authorized administrator of STARS. For more information, please contact STARS@ucf.edu.

STARS Citation

Skaria, Giji, "Studies on Copper Indium based Oxide Transparent Semiconducting Thin Films." (2022). *Electronic Theses and Dissertations, 2020-*. 1091.
<https://stars.library.ucf.edu/etd2020/1091>

STUDIES ON COPPER INDIUM BASED TRANSPARENT
SEMICONDUCTING OXIDE THIN FILMS

by

GIJI SKARIA
M.S. University of Central Florida, 2011

A dissertation submitted in partial fulfillment of the requirements
for the degree of Doctor of Philosophy
in the Department of Electrical and Computer Engineering
in the College of Engineering and Computer Science
at the University of Central Florida
Orlando, Florida

Spring Term
2022

Major Professor: Kalpathy B. Sundaram

© 2022 Giji Skaria

ABSTRACT

Transparent Conducting Oxides (TCOs) have unique optoelectronic properties which allow visible light to pass through while having reasonably high electrical conductivity[1-3]. TCOs find a variety of applications ranging from uses in solar cells, optical displays, reflective coatings, light emission devices, low-emissivity windows, electrochromic mirrors, UV sensors, and windows, defrosting windows, electromagnetic shielding, and transparent electronics. The conductivity of TCOs can be tuned from insulating via semiconducting to conducting as well as their transparency adjusted depending on the donor/acceptor levels as well as the bandgap of the material. This enables the realization of both n-type and p-type TCOs which make them highly attractive for transparent opto-electrical circuitries and technological applications. Most research activities have focused on the optimization of n-type TCOs, but many transparent electronic applications require the necessity of p-type TCOs as well. There is a need to realize p-type TCOs which offer high yield, scalability, and low cost. RF magnetron sputtering of TCO sources can lead to high uniformity and homogeneity, along with the capability to control the film thickness and deposition rate. It also allows for large-area deposition at a relatively low cost and optimum thermal budget.

In this work, we investigate the realization of p-type CuInO_x thin films by RF magnetron sputtering using $\text{Cu}_2\text{O}:\text{In}_2\text{O}_3$ target and study the effects of (i) post-deposition annealing and (ii) substrate heating during a deposition for controlling the optoelectronic and morphological properties. In the first part of the study, post-process annealing of the deposited films was performed at temperatures ranging from 100-900°C in O_2 ambiance. The X-ray diffraction (XRD) analysis performed on the samples identified the presence of $\text{Cu}_2\text{In}_2\text{O}_5$ phases along with CuInO_2 or In_2O_3 for the films annealed above 500°C. A morphological study

performed using SEM shows the crystallization and the grain growth with an increase in the annealing temperatures. Optical studies carried out on the films indicated a small bandgap change in the range of 3.4-3.6 eV during annealing.

In the second part of the study, the effect of substrate heating during the deposition was investigated to reduce the thermal budget of realizing the p-type CuInO_x thin films and also to increase the throughput. It is seen that substrate heating influences the material characteristics more significantly than post-deposition annealing as we can tailor the thin film characteristics in situ to initiate crystalline growth and control the proportion of indium oxide or copper oxide phases to improve the transparency while retaining the p-type characteristics of the thin film. Copper Indium Oxide (CuInO_x) thin films were deposited by the RF magnetron sputtering technique using a $\text{Cu}_2\text{O}:\text{In}_2\text{O}_3$ target at varying substrate temperatures up to 400°C . A morphological study performed using SEM further confirmed the crystallization and the grain growth (95-135 nm) with increasing substrate temperatures resulting in superior conductivity and enhanced transparency of more than 70% in the 400-700 nm range. Optical studies carried out on the films indicated a bandgap change in the range of 2.61-2.99 eV as a function of substrate heating. XPS analysis of the thin films has also been carried out to identify the oxidation state and bonding configurations of Cu, In, and O in copper indium oxide films. Mutually exclusive requirements of having a p-type thin film along with increased conductivity and high transparency were achieved by controlling the migration of indium oxide phases during the sputtering process as verified by the XPS studies. This is due to the controlled replacement of copper sites with indium while maintaining the p-type characteristic of the thin film. Junction studies of the p-type CuInO_x have been investigated with n-Si and ITO for demonstrating heterojunction behavior which can potentially find applications in transparent electronics, photodetectors, and solar cells. A p- CuInO_x /n-Si heterojunction was fabricated

with a measured knee voltage of 0.89V. The photovoltaic behavior of the device was investigated and initial solar cell parameters are reported.

To my Parents

ACKNOWLEDGMENTS

My journey toward the Ph.D. degree in electrical engineering has been taken a long way with lots of valleys and hills, with wrong and good predictions with emerging ideas on different aspects. If I have something to write at this point is not only by my work but the extrovert and unconditional support, guidance, and inspiration from many peoples. I want to take this opportunity to thank these people without whom I would never have come this far professionally and personally.

I would like to express my sincere gratitude to my advisor, Dr. Kalpathy B. Sundaram, for his continuous commitment to helping and supporting me through my graduate career. This dissertation wouldn't have been possible without his guidance and encouragement throughout my study. I also want to thank him for giving me the freedom to go to his office or by phone with any questions or concerns I may have during these periods.

I would also like to thank my committee members, Dr. Jiann-Shiun Yuan, Dr. Reza Abdolvand, Dr. Vikram Kapoor, and Dr. Varadraj Gurupur for their support throughout my years at UCF. They have all helped me on multiple occasions with access to measurement equipment, technical discussions, feedback on research and presentations, as well as joyful conversations.

I would also like to thank my supervisor at work in UCF Dr. Zhihua Qu for his continued support and advise during my time at UCF as the department chair as well as the director of RISES center at UCF.

Special thanks to the staff at AMF and MCF. I am thankful to Mr. Edward Dein for helping me with the cleanroom equipment. I would like to acknowledge the help from Dr. Avra Kundu on

cleanroom-related activities. I would like to thank Mr. Kirk Scammon for helping to take the data from XPS, XRD, EDS, and SEM.

I would like also grateful to my lab mates Dr. Shraddha Dhanraj Nehate, Ashwin Kumar Saikumar, and Sreeram Sundaresh for their help and suggestions during this time. I also would like to thank Ms. Diana Poulalion for her help and support during my MS and Ph.D. degree.

I heartfelt thank you to my dearest Dr. Alexander V Alex uncle and Leela aunty to encourage and support me like my grandfather and grandmother to finish this degree.

An indebted thank you to my dearest friend Mr. Anish George for being one of my pillars of strength and supporting me to succeed in my Ph.D.

I would like to thank my wife Seena Thomas for her support, understanding, and love during all these years. Her support and encouragement were in the end what made this dissertation possible. I would also like to thank my wonderful kids Abel Mathew and Emmanuel Mathew for their patience and sacrifice.

I would like to thank my parents Mr. Mathai Skaria and Annakutty Skaria who were instrumental in shaping me to become the person I am today. Their endless sacrifices allowed me to pursue my dreams. I would like to thank also my brother Mr. Agi Skaria and his wife Suby Baby and their son Milan Agi and their daughter Miveal Anna Agi and my sister Ms. Animol Skaria, her husband Saji Varghese and their son Eldhose Saji and their daughter Anju Saji for supporting me at all the time.

I would also like to thank my parents-in-law Mr. Thomas and Mrs. Chinnamma, and my brothers, sisters, and friends receive my deepest gratitude and love for their dedication, prayer, love, and support during my studies.

Finally, thank you to God for everything.

TABLE OF CONTENTS

LIST OF FIGURES	xii
LIST OF TABLES	xiv
LIST OF ACRONYMS/ABBREVIATIONS	xv
CHAPTER ONE: INTRODUCTION	1
1.1 Copper-Based Delafossite Crystalline Structures	4
1.2 Non-Delafossite Crystalline Structures	5
1.2.1 Orthorhombic crystalline structures.....	6
1.2.2 Spinal crystalline structure.....	6
CHAPTER TWO: LITERATURE REVIEW	8
2.1 Transparent conducting oxides (TCO).....	8
2.2. Indium Tin Oxide (ITO) n-type	10
2.3 P-type TCOs.....	11
2.4 Copper Indium Oxide (CuInO ₂).....	12
CHAPTER THREE: EXPERIMENTAL PROCEDURE.....	14
3.1 Deposition of Copper Indium Oxide Thin Films for Post-Annealing studies.....	14
3.2 Deposition Studies.....	15
3.3 Thickness measurement	20
3.4 Characterization of Post-Annealed Copper Indium Oxide Thin Films.....	21

3.5 Morphological and optical studies of copper indium oxide thin films with substrate heating	23
3.6 Deposition of copper indium oxide thin films with various substrate temperatures.....	26
3.7 Fabrication of CuInO _x heterojunctions and electrical studies	27
CHAPTER FOUR: RESULTS AND DISCUSSIONS.....	28
4.1 Post Annealing Studies.....	28
4.1.1 XRD Analysis	28
4.1.2 Morphology studies	29
4.1.3 Optical Studies	31
4.1.4 Optical Bandgap.....	32
4.2 Substrate Temperature Studies	35
4.2.1 XPS analysis	35
4.2.2 Optical analysis and bandgap.....	36
4.2.3 Morphological studies.....	39
4.3 Heterojunction Studies	40
4.3.1 n-Si/p-CIO heterojunction devices	41
4.3.2 p-CIO/n-ITO heterojunction devices	43
4.3.3 Heterojunction for light characteristic studies	46
CHAPTER FIVE: CONCLUSION.....	49
REFERENCES	51

LIST OF FIGURES

Figure 1: Delafossite crystalline structure	5
Figure 2 orthorhombic crystalline structure.....	6
Figure 3: Spinal crystalline structure	7
Figure 4: RF magnetron sputtering system schematic.....	14
Figure 5: Custom built RF Sputtering, DC Sputtering, and Evaporation system	16
Figure 6: Thickness vs substrate temperature during deposition.....	18
Figure 7: Programmable cube furnace for annealing the samples.....	19
Figure 8: Dektak 150 Profiler to measure the thickness of the deposited thin film	20
Figure 9: PANalytical Empyrean XRD system, Malvern Panalytical, Westborough, MA.....	22
Figure 10: Field emission scanning electron microscope, Zeiss ULTRA-55 FEG SEM, Zeiss Microscopy, White Plains, NY, USA	24
Figure 11 Cary 100 UV–Vis spectrophotometer (Agilent Technologies, Santa Clara, CA, USA)	25
Figure 12 ESCALAB 250 Xi + X-ray photoelectron spectroscopy (XPS)	25
Figure 13: Device schematic for (a) n-Si/p-CIO heterojunction and (b) Quartz p-CIO/n-ITO heterojunction.	27
Figure 14: X-ray diffraction of the films annealed at 500-900°C in O ₂ for 90 minutes	28
Figure 15: SEM images of Cu ₂ In ₂ O ₅ films (a) as-deposited and annealed at (b) 500°C, (c) 600°C, (d) 700°C, (e) 800°C, and (f) 900°C.....	30
Figure 16: Optical transmission spectra of the Cu ₂ In ₂ O ₅ thin films annealed at various temperatures.....	32
Figure 17: Tauc plot of the Cu ₂ In ₂ O ₅ thin films annealed at different temperatures.....	34

Figure 18: (a) XPS spectra of CuInO _x thin films with (b) copper peaks, (c) indium peaks, and (d) oxygen peaks. Figure a-d: (i-iv) correspond to room temperature, 200°C, 300°C, and 400°C respectively	36
Figure 19: (a): Transmittance spectra of CuInO _x films on quartz at different temperatures during deposition. (b) Percentage increase in transmittance for the deposited films due to the effect of substrate heating with respect to room temperature deposition	38
Figure 20: Tauc plots of the CuInO _x thin films deposited at different substrate temperatures	39
Figure 21: (a): SEM images of CuInO _x films on quartz: (a) room temperature, (b) substrate heater temperature of 200°C, (c) substrate heater temperature of 300°C, (d) substrate heater temperature of 400°C.....	40
Figure 22: Fabricated n-Si/p-CIO p-n junction devices.....	41
Figure 23: I-V characteristics (butterfly) of n-Si/p-CIO heterojunction devices.....	42
Figure 24: I-V characteristics (forward) of n-Si/p-CIO heterojunction devices.....	43
Figure 25: Fabricated p-CIO/n-ITO heterojunction devices.....	44
Figure 26: I-V characteristics (butterfly) of p-CIO/n-ITO heterojunction devices	45
Figure 27: I-V characteristics (forward) of p-CIO/n-ITO heterojunction devices	46
Figure 28: Al/n-Silicon/CI/Al heterojunction for light characteristics performance.....	47
Figure 29: Light characteristics	48

LIST OF TABLES

Table 1: A variety of preparation methods and characterization techniques were carried out to develop many TCOs	8
Table 2: Various deposition techniques reported for p-type TCOs	12
Table 3 $\text{Cu}_2\text{In}_2\text{O}_5$ films composition as a function of the annealing temperature, measured in EDAX.	31
Table 4 The extrapolated values of the bandgap for post annealed samples	33
Table 5 The extrapolated values of the bandgap for various substrate temperature.....	38

LIST OF ACRONYMS/ABBREVIATIONS

CIO	Copper Indium Oxide
CuInO ₂ :	Copper Indium Oxide
CuAlO ₂ :	Copper Aluminum Oxide
CuGaO ₂	Copper Gallium Oxide
EDS:	Energy Dispersive Spectroscopy
ITO:	Indium Tin Oxide
PLD:	Pulsed laser deposition
RF	Radio Frequency
RT	Room Temperature
SEM:	Scanning Electron Microscope
SnO ₂	Tin Oxide
TCOs:	Transparent Conducting Oxides
XPS:	X-ray photoelectron spectroscopy
XRD:	X-ray diffraction
ZnO:	Zinc Oxide

CHAPTER ONE: INTRODUCTION

Transparent Conducting Oxides (TCOs) have a unique ability to allow visible light to pass through them with comparably low absorption of electromagnetic waves within the visible region of the spectrum as well as to conduct electricity. TCOs find many applications in solar cells, optical displays, reflective coatings, light emission devices, low-emissivity windows, electrochromic mirrors, UV sensors, and windows, defrosting windows, electromagnetic shielding, and transparent electronics [4-11]. The conductivity of TCOs can be tuned from insulating via semiconducting to conducting as well as their transparency adjusted depending on the donor/acceptor levels as well as the bandgap of the material. This enables the realization of both n-type and p-type TCOs which make them highly attractive for transparent opto-electrical circuitries and technological applications. Most research activities have focused on the optimization of n-type TCOs[12-15]. Well established n-type transparent conducting oxides are $\text{SnO}_2\text{:Sb/F}$, ZnO:In/Al/ F/B/Ga , $\text{In}_2\text{O}_3\text{:Sn/F/Sb/Pb}$, Cd_2SnO_4 etc. Some new n-type TCOs: Zn_2SnO_4 , ZnSnO_3 , $\text{GaInO}_3\text{:Ge/Sn}$, $\text{AgInO}_2\text{:Sn}$, MgIn_2O_4 , $\text{CdSb}_2\text{O}_6\text{:Y}$, $\text{Zn}_2\text{In}_2\text{O}_5$, ZnGa_2O_4 , $\text{In}_4\text{Sn}_3\text{O}_{12}$, $\text{CdIn}_2\text{O}_4\text{:Sn}$ etc. But many transparent electronic applications require the necessity of p-type TCOs as well. Various models have been proposed to obtain new types of p-TCO thin films and a large number of techniques have been adopted to fabricate p-TCO thin films with better electrical and optical properties the maximum conductivity, the conductivity of p-TCO thin films are still one or two orders of magnitude less than the corresponding best n-TCO thin films. Increasing the conductivity of p-TCO thin films without sacrificing their visible transmittance is the most significant challenge for p-TCO technology to obtain high-performance active devices suitable for “Invisible Electronics”[15]. It may be

noted that p-type transparent oxide semiconductors based on CuAlO_2 , CuGaO_2 , CuInO_2 , SrCu_2O_2 , and LaCuOCh (Ch = chalcogen) have been reported[15] Copper indium oxide-copper aluminum oxide and copper gallium oxide-based thin-film materials have emerged as the front runner for possible p-type TCO applications. Of the copper-based systems, the CuInO_2 system is particularly interesting because it can be doped both p-type (with Ca) and n-type (with Sn), allowing p–n homojunction to be produced. Synthesis of $\text{Cu}_2\text{In}_2\text{O}_5$ has been reported only using either smelting[16] or chemical processes, which involve synthesizing $\text{Cu}_2\text{In}_2\text{O}_5$ from aqueous solutions of nitrates, chlorides, and sulfates of Cu, In, and Ga. Therefore, the realization of p-type TCOs has been rather challenging and involves the use of chemicals that present levels of toxicity and low yield or smelting which results in a high thermal budget for the fabricated device.

Transparent conducting oxides with delafossite structure have attracted much attention because of their potential in preparing innovative transparent p-n junctions for these device applications. They are also used as p-type and n-type semiconductive oxides to achieve wide-bandgap p-n junction and devices. The bulk of research done on TCOs involve n-type TCOs [12, 17-24]. Many transparent electronic applications require the necessity of p-type TCOs. There are some research reports on p-type to meet these special types of applications. Researchers are looking at the combination of copper indium oxide (CuInO_2) and copper gallium oxide (CuGaO_2) based on thin-film materials for possible applications [9, 25-34]. Some of the copper-based p-type TCOs are Copper aluminum oxide (CuAlO_2), Copper gallium oxide (CuGaO_2), and Copper indium oxide (CuInO_2). There are some copper-based doped p-type TCOs such as Iron doped copper gallium oxide ($\text{CuGaO}_2\text{:Fe}$), Calcium doped copper indium oxide ($\text{CuInO}_2\text{:Ca}$), and Magnesium doped copper scandium oxide ($\text{CuScO}_2\text{:Mg}$),

Magnesium doped copper chromium oxide ($\text{CuCrO}_2\text{:Mg}$), and Calcium doped copper yttrium oxide ($\text{CuYO}_2\text{:Ca}$).

For the synthesis of transparent conducting oxide thin films and also on device preparation, researchers were working on different kinds of materials like ZnO, CuAlO_2 and SrCuO_2 , etc. Recently, the delafossite oxide of CuInO_2 showed bipolar conductivity with different doping ions. Yanagi et al. reported the preparation of two kinds of CuInO_2 thin films by pulsed laser technique. Unfortunately, PLD is not employed by industries because of the difficulty in scaling up and the low-quality film due to the droplet formation. In this respect, RF magnetron sputtering has several advantages such as high uniformity and homogeneity, capability to control the film thickness and deposition rate, low cost to fabricate, ability to achieve large-area deposition and no toxic gas or chemical in this process. The chemical processes include synthesizing $\text{Cu}_2\text{In}_2\text{O}_5$ from aqueous solutions of nitrates, chlorides, and sulfates of Cu, In, and Ga [31]. At this moment, there have not been many attempts to investigate $\text{Cu}_2\text{In}_2\text{O}_5$ deposited by RF magnetron sputtering. RF Magnetron sputtering allows films to be deposited with high uniformity and homogeneity as well as it provides the capability to control film thickness and deposition rate [35]. It has an additional advantage of low cost and large area deposition. In the first part of this work, the focus has been on the deposition of $\text{Cu}_2\text{In}_2\text{O}_5$ by RF magnetron sputtering using a single target of $\text{Cu}_2\text{O}:\text{In}_2\text{O}_3$ in the ratio of 1:1. The structural and optical properties of $\text{Cu}_2\text{In}_2\text{O}_5$ thin films were investigated.

Nair et al. fabricated a transparent thin-film p–n junction consisting of Ca and tin-doped CuInO_2 [16] by oxygen plasma enhanced reactive thermal evaporation. This allows for scalable physical vapor phase deposition of the desired thin films. Thus, there is a need to realize p-type TCOs which offer high yield, scalability, and low cost. RF magnetron sputtering of TCO

sources, if controlled in situ can lead to high uniformity and homogeneity, along with the capability to control the film thickness and deposition rate. It also allows for large-area deposition at a relatively low cost and optimum thermal budget. In the second part of this work, we investigate the realization of p-type CuInO_x thin films by RF magnetron sputtering and study the effects of substrate heating for in situ controlling of the optoelectronic and morphological properties. It is seen that substrate heating influences the material characteristics more significantly than post-deposition annealing. We can tailor the thin film characteristics in situ to initiate crystalline growth and control the proportion of indium oxide or copper oxide phases to improve the transparency while retaining the p-type characteristics of the thin film at a reduced thermal budget as compared to post-deposition annealing. Scanning electron microscopy imaging has been used to obtain the grain size of the film and UV-Vis spectral measurements have been carried out for transmittance studies. XPS analysis of the thin films has also been carried out to identify the oxidation state and bonding configurations of Cu, In, and O in copper indium oxide films. Junction studies of the p-type CuInO_x have been investigated with n-Si and ITO for demonstrating heterojunction behavior which can potentially find applications in transparent electronics, photodetectors, and solar cells.

1.1 Copper-Based Delafossite Crystalline Structures

Copper-based TCOs have mainly two structures such as delafossite structures and non-delafossite structures. The non-delafossite structures are orthorhombic structures and spinal structures. Figure 1 shows the delafossite crystalline structure of copper indium oxide. The delafossite structure (ABO_2) is characterized by a layer of linearly coordinated A cations stacked between edge-shared octahedral layers (BO_2) where A is the Monovalent cation and B is the trivalent cation. Delafossites are a family of materials having the CuMO_2 formula, where $M = \text{Ga, Al, In, Co, etc}$ [36]. The crystal structure consists of alternating stacks of MO_2

octahedron layers and Cu ion layers. This layered structure leads to highly anisotropic physical properties. The crystal chemistry of the delafossite structure will be discussed about phase stability, the stability of dopants, and important physical properties such as low electrical resistivity (10^{-2} - 10^2 Ω -cm) and high optical transparency due to its high optical bandgap. Delafossite structures are usually synthesized at high temperatures[37-39].

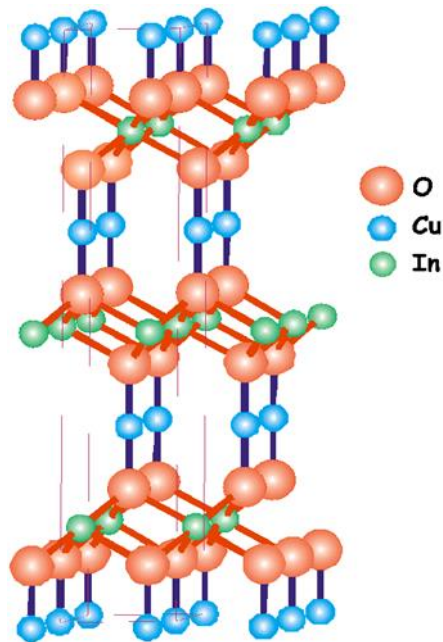


Figure 1: Delafossite crystalline structure

(Alan V Chadwick et al 2010 J. Phys.: Conf. Ser. 249 012045)

1.2 Non-Delafossite Crystalline Structures

There are two types of non-delafossite crystalline structures are found in this type of material such as orthorhombic crystalline structures and spinal crystalline structures.

1.2.1 Orthorhombic crystalline structures

Figure 2 shows the orthorhombic crystalline structures of the copper-based p-type TCOs. The orthorhombic crystalline structures have a formula of $A_2B_2O_5$ where A is the monovalent cation and B is the trivalent cation.

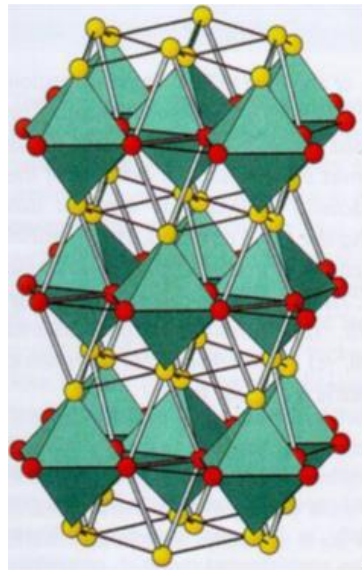


Figure 2 orthorhombic crystalline structure

(Degtyareva, V. (2013). Electronic Origin of the Orthorhombic Cmca Structure in Compressed Elements and Binary Alloys. *Crystals*, 3(3), 419–430)

1.2.2 Spinal crystalline structure

Figure 3 shows the spinal crystalline structure of copper-based transparent conducting oxides. The spinal crystalline structure has the AB_2O_4 formula where A is the monovalent cation and B is the trivalent cation.

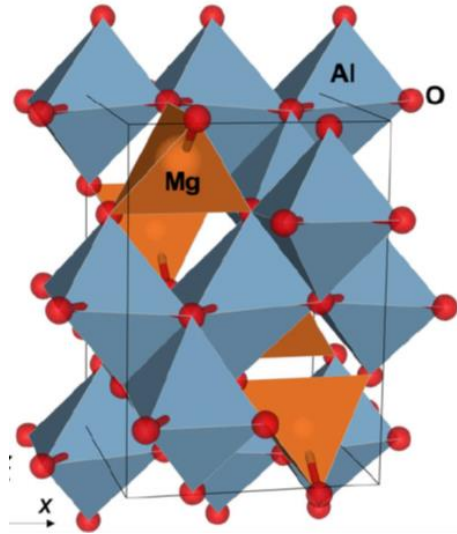


Figure 3: Spinel crystalline structure

(Pilania, G., Kocevski, V., Valdez, J.A. et al. Prediction of structure and cation ordering in an ordered normal-inverse double spinel. *Commun Mater* 1, 84 (2020))

CHAPTER TWO: LITERATURE REVIEW

2.1 Transparent conducting oxides (TCO)

Transparent conducting oxides (TCOs) are high optical transparency and electrically conductive materials with comparable low absorption of electromagnetic waves within the visible region of the spectrum. The requirement should be that more than 80% transmittance in the visible region and low resistivity (10^{-2} - 10^2) Ω cm. TCOs are the compound semiconductors structure of ABO_2 where A, is the monovalent cation and B, is the trivalent cation. The opto-electrical characteristics can be controlled by doping $A_yB_z:D$ (D = dopant), with metals, metalloids, or nonmetals [40].

Table 1 shows the published results regarding the transparent conducting oxides (TCOs) layers. A variety of preparation methods and characterization techniques were carried out to develop many TCOs as shown in Table 1

Table 1: A variety of preparation methods and characterization techniques were carried out to develop many TCOs

Compound semiconductor	Dopant	Preparation	Characterization	Reference
NiO	Li	Pulsed Laser Deposition (Different Li-concentr.)	SEM, XRD, XPS, and Transmission	[41]
ZnO	Na, Al	Sol-gel, Annealing	SEM, Photoluminescence	[42]
Cr ₂ O ₃	Mg, N	Spray Pyrolysis	XRD, Transmittance	[43]

Compound semiconductor	Dopant	Preparation	Characterization	Reference
CuCrO ₂ (Delafossite)	Mg	Sol-gel Technique	SEM, XRD, and Transmission	[44]
Mg _{1-x} Zn _x O	In	Pulsed Laser Deposition (Different substrates)	X-ray diffraction, HRTEM, and Transmission	[45]
Mg _{1-x} Zn _x O	Al	Magnetron Sputtering (different substrates)	X-ray diffraction	[46]
Mg ₁₂ Al ₁₄ O ₃₃ ("Mayenite") Al	In	high-temperature solid- state reaction	X-ray diffraction	[47]
CuAlO ₂		laser ablation	FESEM, X-ray diffraction, and Transmittance	[20]
CuInO ₂	Ca, Sn	oxygen plasma enhanced reactive thermal evaporation	SEM, XRD, XPS, and Transmission	[48]
Cu ₂ In ₂ O ₅		Smelting, chemical, and RF Sputtering	XRD, SEM, and Transmission	[27, 49, 50]
CuGa ₂ O ₄		RF Sputtering	SEM, XRD, XPS, and Transmission	[25]

Outstanding characteristics were provided by zinc, indium, and tin oxides. A well-known TCO is Indium tin oxide (ITO) and the doping of zinc oxide with less than 5% Al (ZnO: Al) was established in 1954. Some applications of transparent conducting oxides are Solar cells, Front electrodes in flat panel displays, Optical displays, Reflective coatings, Light emission devices,

Low-emissivity windows, Smart windows, Electrochromic mirrors (rearview mirrors), UV sensors, touch-sensitive control panels, Windows/defrosting windows, Electromagnetic shielding, Transparent electronics, Invisible security circuits, Gas sensors, Biosensors, Antistatic coatings, and Cold heat mirrors, etc. Most of the widely used oxide-based TCOs are n-type conductors that ideally have a wide bandgap of >3 eV, the ability to be doped to dissoluteness, and an electron-effective mass that ensures that the plasma absorption edge lies in the infrared range. ITO is the most widely used TCOs in optoelectronic devices. The transparent conductor must be cautiously processed to maximize optical transmissivity in the visible spectra while attaining minimum electrical resistivity for use in optoelectronic applications. There are two types of TCOs such as n-type TCOs and p-type TCOs. Well-known and widely available n-type TCOs with low resistivity of 10^{-3} Ω cm are $\text{SnO}_2\text{:Sb/F}$, ZnO: In/Al/F/B/Ga , $\text{In}_2\text{O}_3\text{:Sn/F/Sb/Pb}$, Cd_2SnO_4 , etc. Some new n-type TCOs are such as Zn_2SnO_4 , ZnSnO_3 , $\text{GaInO}_3\text{:Ge/Sn}$, $\text{AgInO}_2\text{:Sn}$, MgIn_2O_4 , $\text{CdSb}_2\text{O}_6\text{:Y}$, $\text{Zn}_2\text{In}_2\text{O}_5$, ZnGa_2O_4 , $\text{In}_4\text{Sn}_3\text{O}_{12}$, $\text{CdIn}_2\text{O}_4\text{:Sn}$ etc.

2.2. Indium Tin Oxide (ITO) n-type

Indium tin oxide is an n-type TCO that is widely used for TCO applications such as solar cells, flat panel displays, touch displays, smart windows, electrochromic mirrors, etc. Indium tin oxide (ITO) is a ternary composition of indium, tin, and oxygen in varying proportions. The ITO can be identified as either ceramic or alloy depending upon the oxygen content. Typically, ITO comes across as an oxygen-saturated composition with a preparation of 74% In, 18% Sn, and 8% O by weight. Oxygen-saturated compositions are so typical that unsaturated compositions are termed oxygen-deficient ITO. It is transparent and colorless in thin layers, while in the bulk form it is yellowish to gray. In the infrared region of the spectrum, it acts as a metal-like mirror. ITO films are the most commonly used n-type transparent

conducting thin films for transparent oxide applications due to their high electrical conductivity and very good optical transparency. Indium tin oxide (ITO) is an optoelectronic material that is applied widely in both research and industry. ITO can be used for several applications, such as flat-panel displays, smart windows, polymer-based electronics, thin-film photovoltaics, glass doors of supermarket freezers, and architectural windows. In this work, I used ITO as the n-type TCO to make p-n heterojunction.

2.3 P-type TCOs

Although the transparent conducting oxides have a massive range of applications as mentioned above, very little work has been done on active device fabrication using TCOs. The reason behind this is because that most of the above-mentioned TCOs are n-type semiconductors. Nevertheless, the consistent p-type transparent conducting oxides (p-TCO), which are essential for junction devices, were unexpectedly missing in thin-film form for a long time until in 1997, Kawazoe et al. from Tokyo Institute of Technology, Japan, reported p-type conductivity in a highly transparent thin film of copper aluminum oxide (CuAlO_{2+x}) [20]. This provides an opportunity to make transparent active devices for Transparent Electronics applications. Copper based p-type TCOs are Copper aluminum oxide (CuAlO_2), Copper gallium oxide (CuGaO_2), and Copper indium oxide (CuInO_2). Doped versions of some p-TCOs are Iron doped copper gallium oxide ($\text{CuGaO}_2:\text{Fe}$), Calcium doped copper indium oxide ($\text{CuInO}_2:\text{Ca}$), and Magnesium doped copper scandium oxide ($\text{CuScO}_2:\text{Mg}$), Magnesium doped copper chromium oxide ($\text{CuCrO}_2:\text{Mg}$), and Calcium doped copper yttrium oxide ($\text{CuYO}_2:\text{Ca}$). Table 2 shows the various deposition techniques reported for p-type TCOs.

Table 2: Various deposition techniques reported for p-type TCOs

Deposition technique	p-type TCOs
Pulsed laser deposition	CuAlO ₂ , CuGaO ₂ , CuInO ₂ :Ca, CuScO ₂ , Cu ₂ SrO ₂ , ZnO:N
R.F. magnetron Sputtering	CuAlO ₂ , CuGa _{0.5} Fe _{0.5} O ₂ , CuCr _{0.95} Mg _{0.05} O ₂ , CuScO _{2+y} , CuSc _{0.95} Mg _{0.05} O ₂ , CuNi _{0.67} Sb _{0.33} Sn _{0.033} O ₂ , AgCoO ₂ , NiCo ₂ O ₄ , (LaO)CuS, (La _{1-x} Sr _x O)CuS, In ₂ O ₃ eAg ₂ O, Cu ₂ BaS ₂ , CuGa ₂ O ₄ ,
D.C. Sputtering	CuAlO ₂
Chemical vapor deposition	CuAlO ₂ , ZnO:N
Sol-gel Technique	CuCrO ₂
laser ablation	CuAlO ₂
oxygen plasma enhanced reactive thermal evaporation	CuInO ₂
Smelting, chemical process	Cu ₂ In ₂ O ₅

2.4 Copper Indium Oxide (CuInO₂)

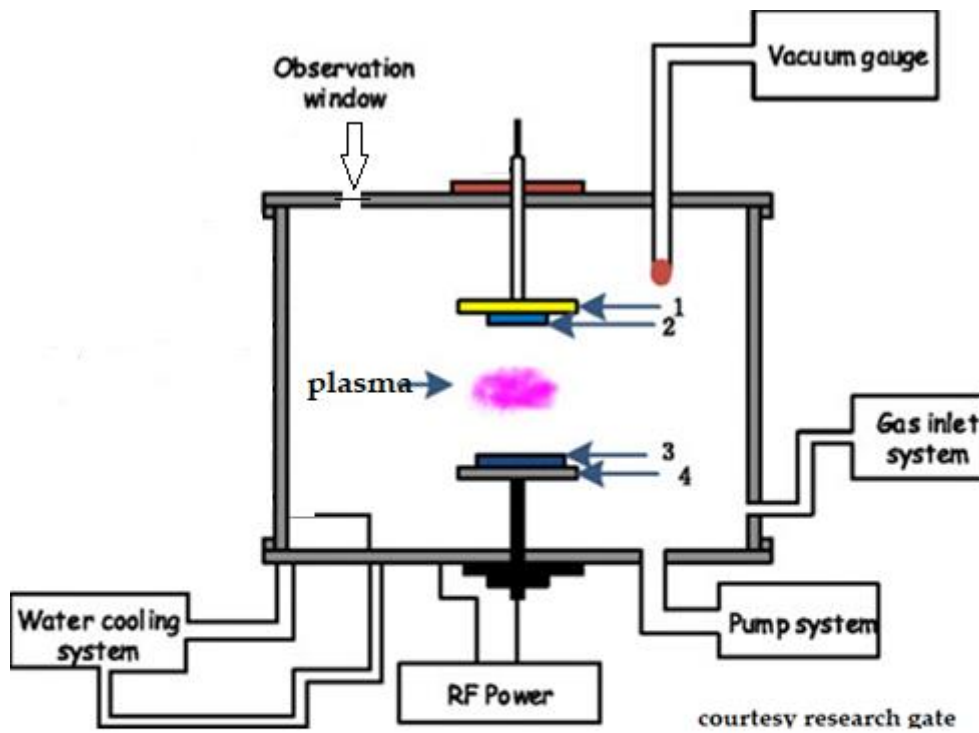
The realization of low resistive high transparency p-type TCOs will increase the usage of these materials as the active semiconductors for transparent heterojunction fabrications. Copper-based TCOs have the unique property of good conductivity, good transparency, and high optical bandgap. To achieve the CIO delafossite structure, the process has to be tailored. A very high-temperature process is required to obtain high transparency while maintaining the p-type behavior. Of the copper-based systems, the CuInO₂ system is particularly interesting because it can be doped with both p-type (with Ca) and n-type (with Sn), allowing p-n

homojunction to be produced. The synthesis of $\text{Cu}_2\text{In}_2\text{O}_5$ has been reported only using either smelting [49] or chemical processes, which involve synthesizing $\text{Cu}_2\text{In}_2\text{O}_5$ from aqueous solutions of nitrates, chlorides, and sulfates of Cu, In, and Ga [27]. Therefore, the realization of p-type TCOs has been rather challenging and involves the use of chemicals that present levels of toxicity and low yield or smelting which results in a high thermal budget for the fabricated device.

CHAPTER THREE: EXPERIMENTAL PROCEDURE

3.1 Deposition of Copper Indium Oxide Thin Films for Post-Annealing studies

Figure 4 shows the schematic diagram of the RF magnetron sputtering system.



- 1- Substrate holder
- 2- Substrate
- 3- Target
- 4- Sputtering Gun

Figure 4: RF magnetron sputtering system schematic

3.2 Deposition Studies

RF magnetron sputtering of copper indium oxide thin films was done on several glass samples to find the deposition rate. The best deposition rate was identified and it follows.

- Base pressure : 5×10^{-6} Torr
- RF Power : 50 W
- Inert gas : Argon
- Argon flow rate : 10 sccm
- Deposition pressure : 10 mTorr
- Substrate temperature : Room temperature
- Distance from target to substrate : 5 cm
- Deposition time : 7.5 minutes (270Å/minute)
- Thickness : Approximately 2000 Å

Figure 5 shows the custom build RF sputtering system capable of doing thermal evaporation and DC sputtering features. The main advantages of using RF magnetron sputtering to deposit the copper indium oxide thin films such as the high uniformity and homogeneity, and the capability to control the film thickness and deposition rate. It also can achieve large-area deposition as well as the low cost are the main advantages to use the RF magnetron sputtering technique.



Figure 5: Custom built RF Sputtering, DC Sputtering, and Evaporation system

Copper indium oxide films were deposited by a radio frequency magnetron sputtering system using a CTI 100 cryogenic high-vacuum pump. A 600 W, 13.56 MHz RF power supply (Dressler Cesar 136 FST RF Generator, Denver, CO, USA) was used to power the MAK 2 sputter gun (San Jose, CA, USA). The Advance Energy VarioMatch-1000 matching network (Fort Collins, CO, USA) was used to match the source and the load impedance. All the depositions were performed at a power of 50 W. The power was ramped up at the rate of 1 W/s. Glass substrates were used to deposit the films for annealing studies up to 400°C, whereas quartz substrates were used for annealing studies above 500°C. The substrates were cleaned with acetone and methanol in an ultrasonic bath followed by rinsing using DI water. The samples were dried with nitrogen gas before loading them into the vacuum system. A 2” powder pressed target of $\text{Cu}_2\text{O}/\text{In}_2\text{O}_3$ (1/1 mol%, 99.9% purity), ACI Alloy Inc. (San Jose, CA,

USA), was used to deposit the films. A gap of 5 cm between the target and the substrate was maintained to achieve a uniform film thickness.

A base pressure of 5×10^{-6} Torr was achieved before initiating the deposition. During the deposition, the pressure was maintained at 10 mTorr with an argon flow of 10 sccm. The deposition rate was found to be approximately 270 Å per minute. This was measured using a Veeco Dektak-150 profilometer (Plainview, NY, USA). All the depositions were conducted for 7.5 min to achieve approximately 2000 Å of film thickness. Post-deposition annealing was conducted from 100 to 900°C for 90 min in O₂ gas flow. Figure 7 shows the cube furnace used for annealing the samples.

A deposition study was also performed with different substrate temperatures during deposition. The deposition was done at room temperature, 100°C, 200°C, 300°C, and 400°C respectively. The deposition conditions are as follows.

- Base pressure : 5×10^{-6} Torr
- RF Power : 100 W
- Inert gas : Argon
- Argon flow rate : 10 sccm
- Deposition pressure : 10 mTorr
- Substrate temperature : RT, 100°C, 200°C, 300°C, and 400°C
- Distance from target to substrate : 5 cm
- Deposition time : 5 minutes

All the deposited films were measured in Veeco Dektak 150 Profiler to find the step height (Thickness of the thin film). Figure 6 shows the thickness of the obtained films after 5 minutes of deposition at varying substrate temperatures. It is seen that the final thickness obtained at

higher temperatures reduces which may be attributed to higher thin film densities and lower porosities. It is interesting to point out here that the substrate temperature also increases due to collisions from secondary electrons.

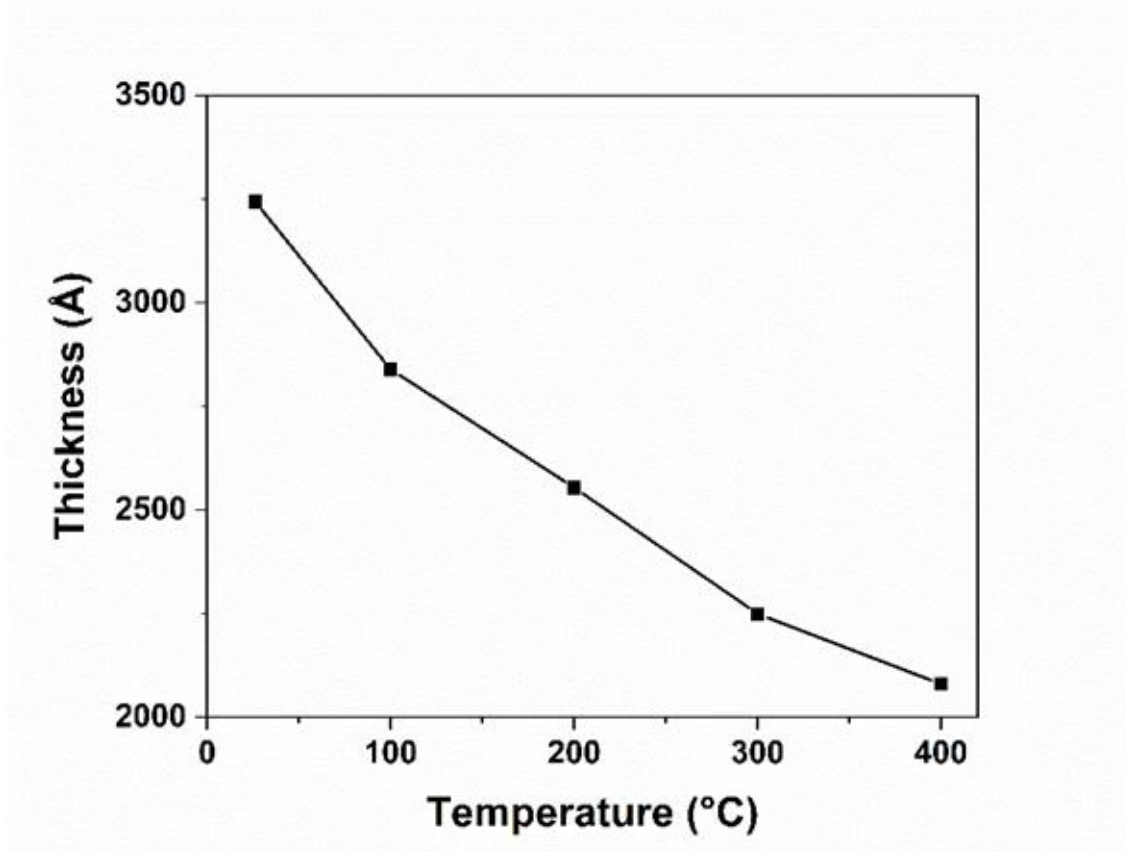


Figure 6: Thickness vs substrate temperature during deposition.



Figure 7: Programmable cube furnace for annealing the samples

3.3 Thickness measurement

All the deposited films were measured using Dektak 150 profiler (figure 8) to identify the thickness of the thin film deposited. To find the thickness of the film and the deposition rate, mark a wide line using a sharpie before the deposition study sample is loaded into the chamber. The samples were cleaned with acetone to remove the marked area to remove the film and cleaned with water and dried with N_2 . All the samples were measured in hill-valley configuration with 10mg stylus force in 30 seconds scan length to find the thickness of the deposited film.



Figure 8: Dektak 150 Profiler to measure the thickness of the deposited thin film

3.4 Characterization of Post-Annealed Copper Indium Oxide Thin Films

The XRD measurements were performed using a PANalytical Empyrean XRD system (Malvern Panalytical, Westborough, MA, USA), using radiation from a Cu source at 45 kV and 40 mA. Figure 9 shows the actual XRD system which used to do X-ray diffraction of the annealed samples. The diffraction patterns were recorded between 2θ angles of 15° and 60° , and the phase information was analyzed using HighScore Plus software (Malvern Panalytical, Westborough, MA, USA). The surface morphology of the film was assessed using a field-emission scanning electron microscope, Zeiss ULTRA-55 FEG SEM (Zeiss Microscopy, White Plains, NY, USA). The optical transmission studies were performed using a Cary 100 UV–Vis spectrophotometer (Varian Analytical Instruments, Walnut Creek, CA, USA).



Figure 9: PANalytical Empyrean XRD system, Malvern Panalytical, Westborough, MA

USA

3.5 Morphological and optical studies of copper indium oxide thin films with substrate heating

The surface morphology of the film was assessed using a field emission scanning electron microscope, Zeiss ULTRA-55 FEG SEM (Zeiss Microscopy, White Plains, NY, USA). Figure 10 shows the actual Scanning Electron Microscope used for the morphological studies. The optical transmission studies were performed using a Cary 100 UV–Vis spectrophotometer (Varian Analytical Instruments, Walnut Creek, CA, USA). Figure 11 shows the UV visible spectrophotometer to find the transmission of the annealed samples. The composition of the films was determined using ESCALAB 250 Xi + X-ray photoelectron spectroscopy (XPS) by Thermo Fisher Scientific with a monochromatic Al K α source (1486.7 eV). Figure 12 shows the actual X-ray photoelectron spectroscopy used to do the XPS analysis. To remove the surface oxygen, an in-built monatomic EX06 ion source was used to perform ion milling of the film surface before XPS measurements. Thermo Fischer Scientific Avantage (software version 5.9902) was used to identify elemental composition and fit the XPS peaks. A smart Shirley function was used to subtract the background for the XPS spectra. The peak fitting was performed by using a mixed Gaussian/Lorentzian function after background subtraction.

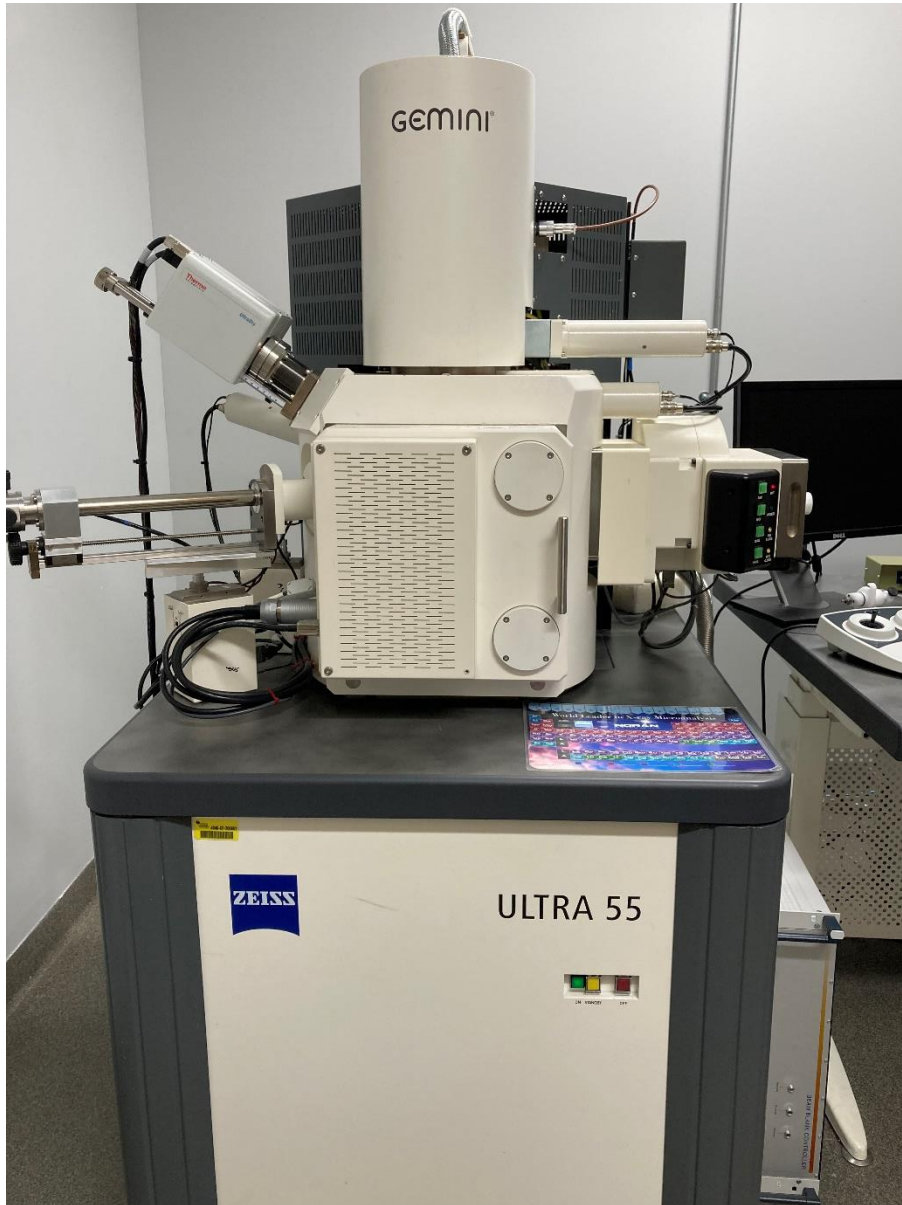


Figure 10: Field emission scanning electron microscope, Zeiss ULTRA-55 FEG SEM, Zeiss Microscopy, White Plains, NY, USA



Figure 11 Cary 100 UV–Vis spectrophotometer (Agilent Technologies, Santa Clara, CA, USA)

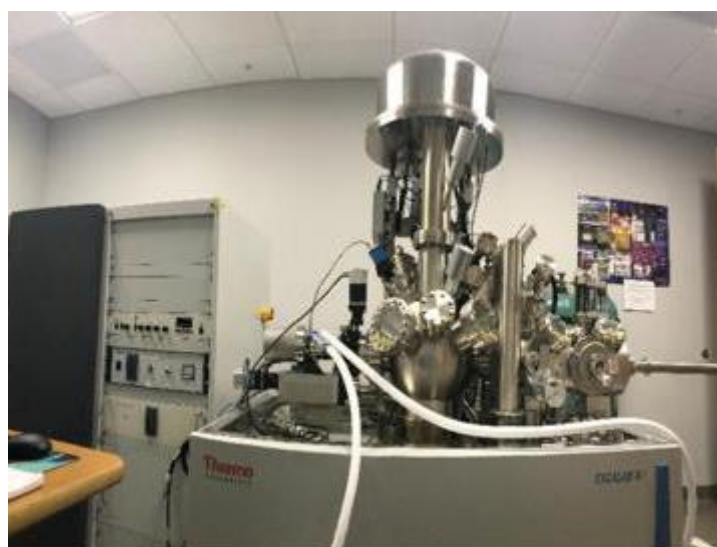


Figure 12 ESCALAB 250 Xi + X-ray photoelectron spectroscopy (XPS)

3.6 Deposition of copper indium oxide thin films with various substrate temperatures

Copper indium oxide films were deposited by a radio frequency magnetron sputtering system using a CTI 100 cryogenic high-vacuum pump. A 600 W, 13.56 MHz RF power supply (Dressler Cesar 136 FST RF Generator, Denver, CO, USA) was used to power the MAK 2 sputter gun (San Jose, CA, USA). The Advance Energy VarioMatch-1000 matching network (Fort Collins, CO, USA) was used to match the source and the load impedance. During the deposition, the pressure was maintained at 10 mTorr with an argon flow of 10 sccm. All the depositions were performed at a power of 100 W. The power was ramped up at the rate of 1 W/s. Quartz substrates were used to deposit the films. The substrates were cleaned with acetone and methanol in an ultrasonic bath followed by rinsing using DI water. The samples were dried with nitrogen gas before loading them into the vacuum system. A 2" powder pressed target of $\text{Cu}_2\text{O}/\text{In}_2\text{O}_3$ (1/1 mol%, 99.9% purity), ACI Alloy Inc. (San Jose, CA, USA), was used to deposit the films. Highly dense single-phase targets for CuInO_2 thin film growing are still challenging, therefore a $\text{Cu}_2\text{O}-\text{In}_2\text{O}_3$ composite target instead of a CuInO_2 single-phase target was used in this study. Further, having the composite target allows for more flexibility in controlling the Cu_2O and In_2O_3 phases in the deposited thin film. A gap of 5 cm between the target and the substrate was maintained to achieve a uniform film thickness. A base pressure of 5×10^{-6} Torr was achieved before initiating the deposition. The deposition rate was found to be approximately 270 Å per minute. This was measured using a Veeco Dektak-150 profilometer (Plainview, NY, USA).

3.7 Fabrication of CuInO_x heterojunctions and electrical studies

(a) 1-20 Ω -cm n-type silicon was used to fabricate the Si heterojunctions. Aluminum as the contact for the n-type silicon was deposited on the backside of the silicon using the thermal evaporation technique. Post annealing at 400°C for 30 minutes in N₂ ambiance was conducted before depositing the CuInO_x thin films. Figure 13 (a) shows the structure of the fabricated device.

(b) A quartz substrate was used to fabricate the heterojunction on a transparent platform. 4000 Å of copper indium oxide films were deposited with a substrate temperature of 400°C. 1 cm x 1 cm area was opened and the rest of the area was masked using aluminum foil and indium tin oxide was deposited by RF magnetron sputtering (100 W, 10 mTorr, 10 sccm Ar) at room temperature (RT) to obtain a thickness of 4000 Å. A mask with several holes (1 mm diameter) is used to deposit aluminum contacts on copper indium oxide (p-type) as well as indium tin oxide (n-type). Figure 13 (b) shows the structure of the fabricated device.

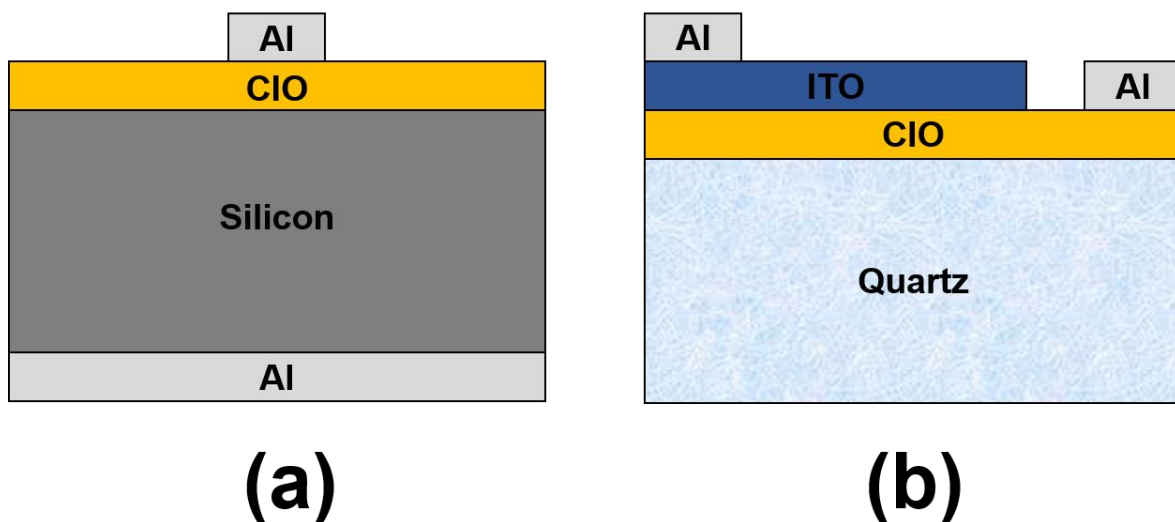


Figure 13: Device schematic for (a) n-Si/p-CuInO_x heterojunction and (b) Quartz p-CuInO_x/n-ITO heterojunction.

CHAPTER FOUR: RESULTS AND DISCUSSIONS

4.1 Post Annealing Studies

4.1.1 XRD Analysis

As-deposited films and films annealed up to 400°C did not reveal any diffraction peaks indicating an amorphous nature. Although the XRD measurement was conducted between 15° and 60°, due to the presence of a broad amorphous peak related to the quartz substrates, the 2θ angle reported in Figure 14 is limited between 25° and 60°.

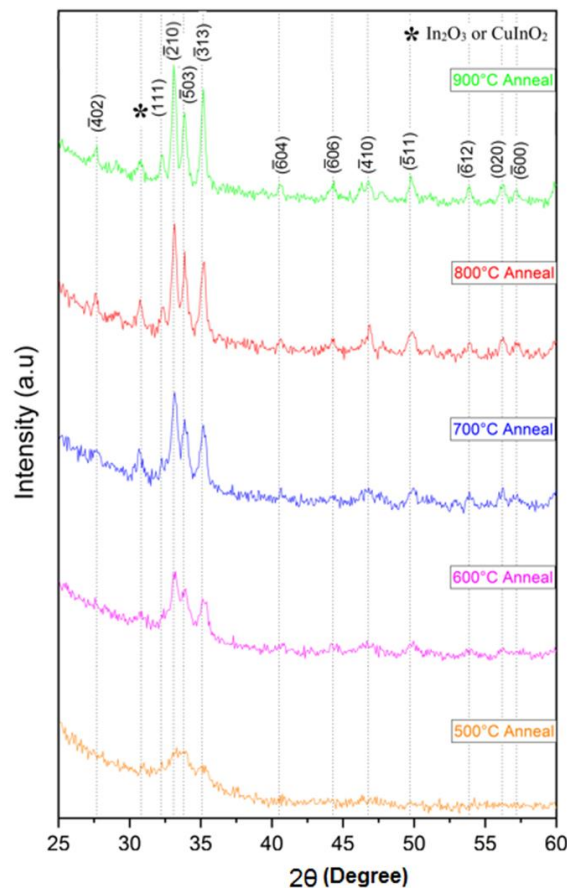


Figure 14: X-ray diffraction of the films annealed at 500-900°C in O₂ for 90 minutes

Figure 14 shows the X-ray diffractograms of the films annealed at 500–900°C in an O₂ atmosphere. The film annealed at 500°C started showing low-intensity peaks related to the

$(\bar{2}10)$, $(\bar{5}03)$, and $(\bar{3}13)$ planes that have been attributed to the $\text{Cu}_2\text{In}_2\text{O}_5$ phase (JCPDS PDF# 30-0479). The films annealed at 600°C and above showed more peaks related to $\text{Cu}_2\text{In}_2\text{O}_5$. It was observed that the peak intensity and peak sharpness increased with an increase in annealing temperature, denoting an increase in crystallinity. These identified planes match very well with the $\text{Cu}_2\text{In}_2\text{O}_5$ -synthesized nanoparticles reported by Su et al. [20]. In addition to the $\text{Cu}_2\text{In}_2\text{O}_5$ phase, a peak at 30.7° (006) was identified. This can be attributed to either the In_2O_3 or CuInO_2 phase [31]. As-deposited films (not shown in Figure 14) did not display any diffraction peaks.

The grain size of the films annealed at 500-900°C was calculated using the Debye-Scherrer equation (equation 1) [32].

$$D = \frac{0.9\lambda}{\beta \cos \theta} \quad (1)$$

Where θ is the Bragg angle, β is the full width at half the maximum peak, λ is the wavelength of the X-ray, and D is the average grain size. The $(\bar{3}13)$ peak was used for the calculation of grain size. The average grain size of the $\text{Cu}_2\text{In}_2\text{O}_5$ films annealed at 500, 600, 700, 800, and 900°C were calculated to be 10, 13, 17, 21, and 27nm respectively.

4.1.2 Morphology studies

Figure 15 shows the SEM images of as-deposited $\text{Cu}_2\text{In}_2\text{O}_5$ thin films as well as those annealed at a temperature varying from 500 to 900°C. Changes in the morphology were identified for the films annealed at 500-900°C. As-deposited films and the film annealed at 500°C displayed the presence of very small grains, as shown in figure 15 a and b. However, the film annealed at 600°C and above showed an increase in grain size. This coincided with the results from the XRD analysis where the diffraction peaks started to appear for films annealed at 500°C and above. Both the SEM and the XRD analysis studies indicated that a minimum of 500°C is required to initiate nanocrystalline growth. Continuous growth in grain size was subsequently

observed for the films annealed at 600–900°C. It is worth mentioning that a pinhole-like appearance was detected in films annealed at 800 and 900°C. Elemental analysis of all the samples was performed using EDAX incorporated in the FESEM. Nearly equal ratios of Cu: In were identified in all films. Table 3 shows the $\text{Cu}_2\text{In}_2\text{O}_5$ films composition as a function of the annealing temperature.

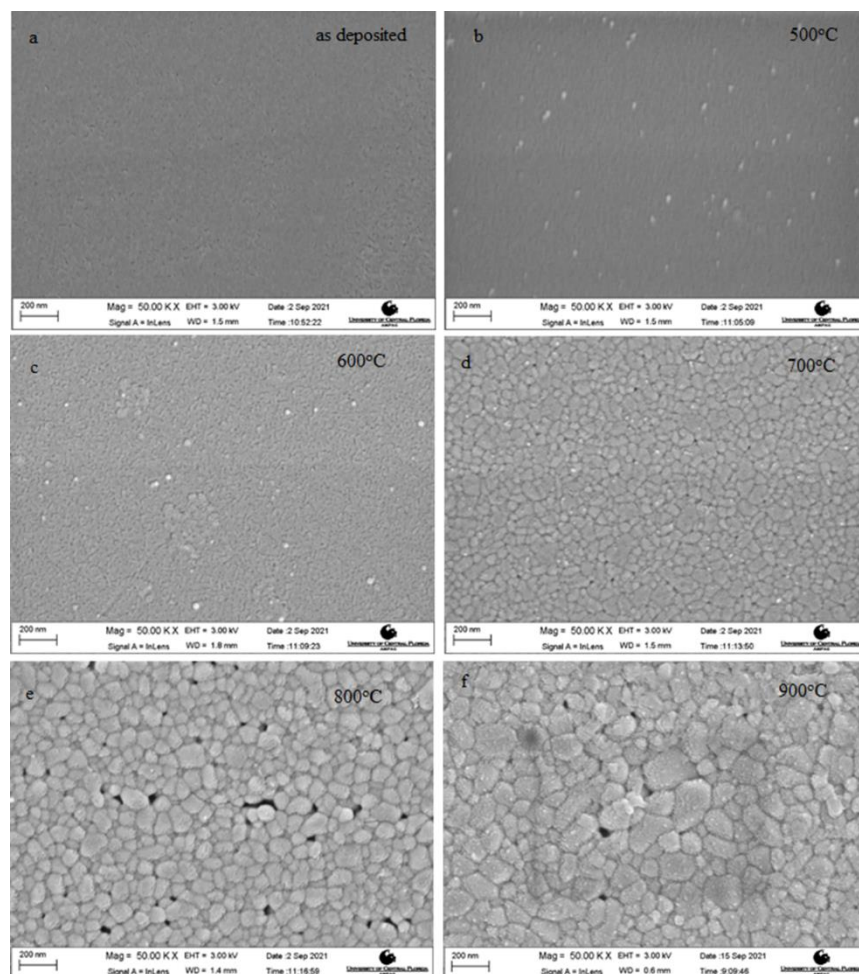


Figure 15: SEM images of $\text{Cu}_2\text{In}_2\text{O}_5$ films (a) as-deposited and annealed at (b) 500°C, (c) 600°C, (d) 700°C, (e) 800°C, and (f) 900°C

Table 3 Cu₂In₂O₅ films composition as a function of the annealing temperature, measured in EDAX.

Film	Cu atm %	In atm %	O atm %
As deposited	13.0	11.3	75.7
Annealed at 500°C	12.6	12.7	74.7
Annealed at 600°C	13.7	14.7	71.6
Annealed at 700°C	13.8	14.1	72.1
Annealed at 800°C	14.6	14.9	70.4
Annealed at 900°C	15.4	14.0	70.6

4.1.3 Optical Studies

A Cary 100 UV–Vis spectrophotometer (Figure 11: Agilent Technologies, Santa Clara, CA, USA) was used to perform the optical characterization of the annealed Cu₂In₂O₅ thin films. Figure 16 shows the percent of transmission for the films deposited on glass and quartz substrates and subsequently annealed from 100 to 900°C. Overall, the optical transmission increased for the films annealed at different temperatures. The transmission values of the annealed films were observed to vary between 70% and 90%. At a 450 nm wavelength, the films annealed at 900°C displayed the highest transmission of 80%. However, the films annealed at 900°C subsequently showed a decreasing trend in transmission beyond a 500 nm wavelength. This could be attributed to an increase in grain size with annealing, as reported in [33,34].

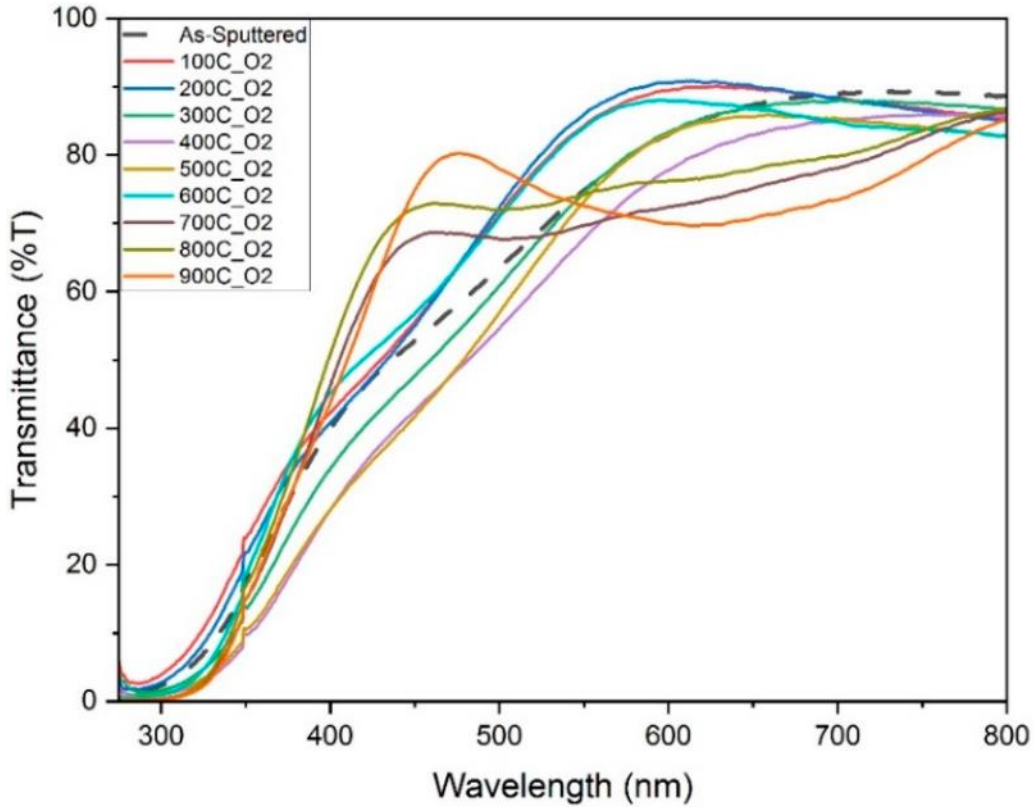


Figure 16: Optical transmission spectra of the $\text{Cu}_2\text{In}_2\text{O}_5$ thin films annealed at various temperatures.

4.1.4 Optical Bandgap

The optical transmission data were used to calculate the optical band gap of $\text{Cu}_2\text{In}_2\text{O}_5$ thin films using the Tauc plot method [35–37]. Since the reflectance was identified to be less than 5%, the absorption coefficient α was calculated directly from the transmission data [36]. The absorption coefficient α was calculated using Equation (2), where d is the thickness of the film, and T is the percent of transmission. The optical bandgap (E_g) was estimated from Equation (3).

$$\alpha = \frac{1}{d} \ln\left(\frac{1}{T}\right) \quad (2)$$

$$(\alpha h\nu)^{1/n} = B(h\nu - E_g) \quad (3)$$

Where $h\nu$ is the photon energy, B is a constant and E_g is the optical bandgap, and $n=1/2$ for the direct bandgap transition. Figure 17 a-j shows the Tauc plot generated using the above equations. The linear region of the curve was extrapolated to the x-axis to identify the E_g value. The extrapolated values of the bandgap are listed in Table 4. The bandgap was reported for the first time in this work for $\text{Cu}_2\text{In}_2\text{O}_5$ thin films. The bandgap was in the range of 3.4-3.6 eV. It is worth mentioning that an increase in annealing temperature did not have any major effect on the bandgap.

Table 4 The extrapolated values of the bandgap for post annealed samples

Annealing temperature (°C)	Bandgap (eV)
As dep	3.59
100	3.45
200	3.6
300	3.54
400	3.48
500	3.53
600	3.66
700	3.66
800	3.66
900	3.64

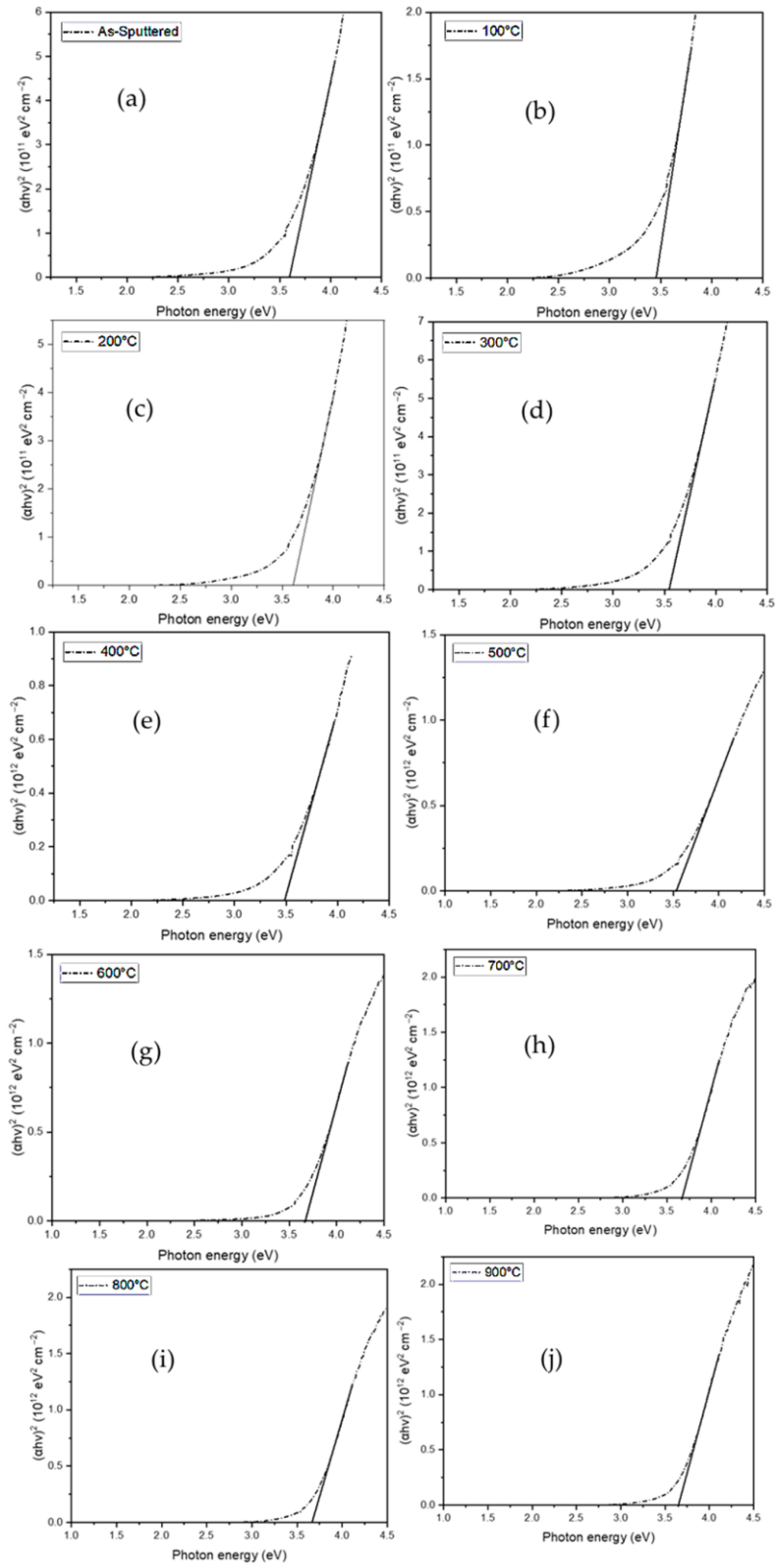


Figure 17: Tauc plot of the $\text{Cu}_2\text{In}_2\text{O}_5$ thin films annealed at different temperatures

4.2 Substrate Temperature Studies

4.2.1 XPS analysis

Figure 18 (a: i-iv) shows the XPS spectra obtained from the CuInO_x films sputtered at room temperature, 200°C, 300°C, and 400°C respectively. Peaks pertaining to only Cu, In, and O were identified in the obtained XPS survey spectra shown in Fig. 18 (a: i-iv), thereby confirming the phase purity. From Figure 18 (b:i-iv), two strong peaks are obtained at 933.8 eV and 953.7 eV, belonging to $\text{Cu } 2p_{3/2}$ and $\text{Cu } 2p_{1/2}$, respectively [18]. The presence of Cu^{2+} species was confirmed by the satellite peaks between 940 and 950 eV. Figure 18 (c: i-iv) shows the $3d_{5/2}$ and $3d_{3/2}$ indium core levels observed at a binding energy of 444.1 eV and 451.7 eV [18]. Oxygen 1s core level Figure 18 (d: i-iv) has been fitted with three Gaussian peaks located at 529.5 eV, 531.3 eV, and 532.5 eV (marked 1, 2, and 3), respectively. Peak 1 is attributed to oxygen attached to In (+3) while peak 2 is attributed to oxygen attached to Cu (+1). Peak 3 is attributed to strongly chemisorbed oxygen which is normally observed at 532.2 eV [18]. It is seen from Figure 18 (d: i-iv) that the strength of peak 2 reduces relative to that of peak 1. This indicates that there is a controlled addition of indium oxide phases to the thin film as a result of substrate heating while maintaining sufficient copper oxide phases. The addition of the indium oxide phases causes the thin film to become more transparent while the optimal presence of copper oxide phases enables the film to retain its p-type characteristics. This is also validated by the transmittance measurements for transparency as well as hot probe measurements for the p-type behavior [16].

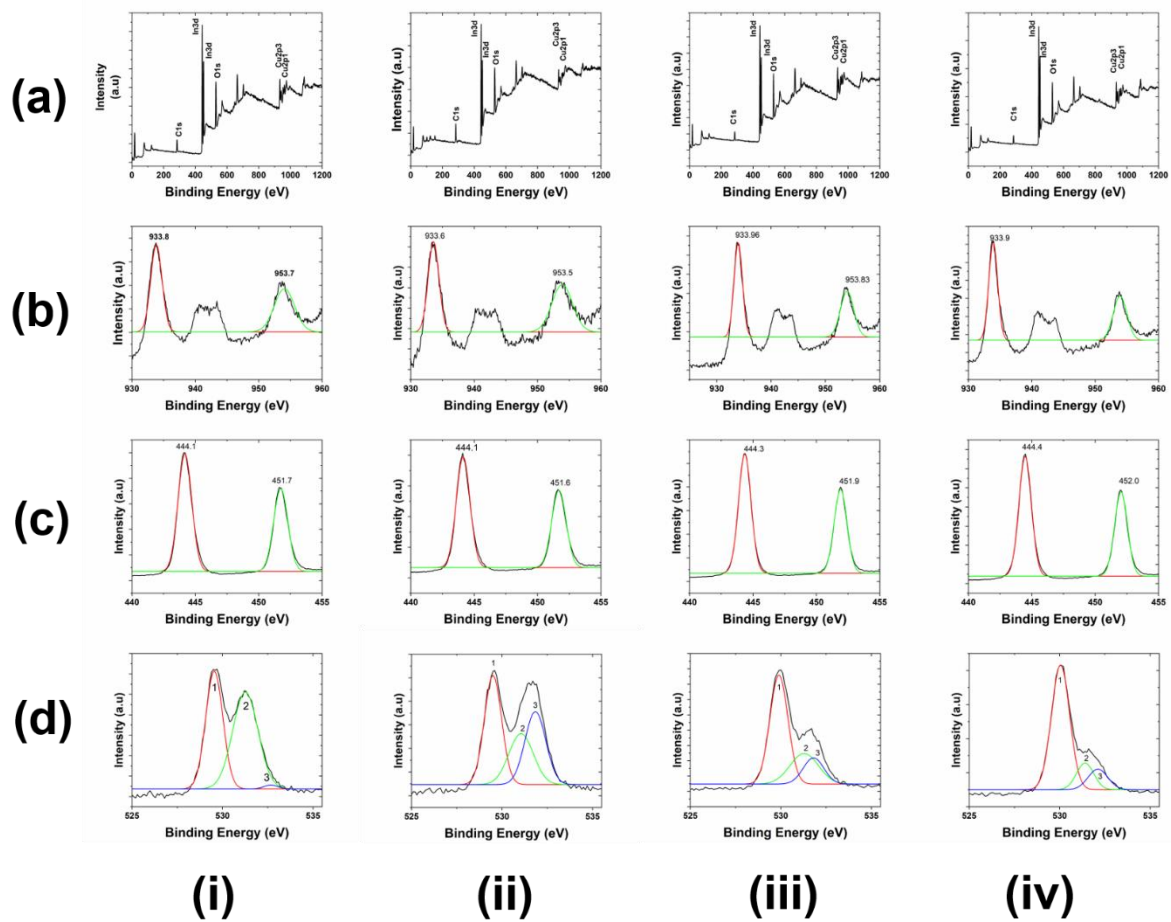


Figure 18: (a) XPS spectra of CuInOx thin films with (b) copper peaks, (c) indium peaks, and (d) oxygen peaks. Figure a-d: (i-iv) correspond to room temperature, 200°C, 300°C, and 400°C respectively

4.2.2 Optical analysis and bandgap

Figure 19 (a) shows the percentage transmission in 300 – 800nm wavelength for the films deposited on quartz substrates at room temperature, 200°C, 300°C, and 400°C. Overall, the optical transmission increases for the films deposited at higher temperatures. This is because of the controlled addition of the indium oxide phases at the copper oxide sites as already verified by the XPS analysis. It is seen that the percentage increase in transmittance varies up to 25-100% between 400-700 nm wavelength for substrate temperature of 400°C. Figure 19(b)

shows the percentage increase in transmittance for the deposited films due to the effect of substrate heating with respect to room temperature deposition between 400-700 nm wavelength. The optical transmission data were used to calculate the optical band gap of CuInO_x thin films using the Tauc plot method [51, 52]. Since the reflectance was identified to be less than 5%, the absorption coefficient α was calculated directly from the transmission data. The absorption coefficient α was calculated using Equation (4), where d is the thickness of the film, and T is the percent of transmission. The optical bandgap (E_g) was estimated from Equation (5).

$$\alpha = \frac{1}{d} \ln \left(\frac{1}{T} \right) \dots \quad (4)$$

$$(\alpha h\nu)^{1/n} = B (h\nu - E_g) \dots \quad (5)$$

where $h\nu$ is the photon energy, B is a constant, E_g is the optical bandgap, and $n = 1/2$ for the direct bandgap transition. Figure 20 shows the Tauc plot generated using the above equations. The linear region of the curve was extrapolated to the x-axis to identify the E_g value. The extrapolated values of the bandgap are listed in Figure 20. The bandgap was in the range of 2.52–2.99 eV. Table 5 shows the bandgap values of the sample deposited in various substrate temperature. It is worth mentioning that an increase in the bandgap is also attributed to the addition of the indium oxide phases as it has a higher bandgap than copper oxide.

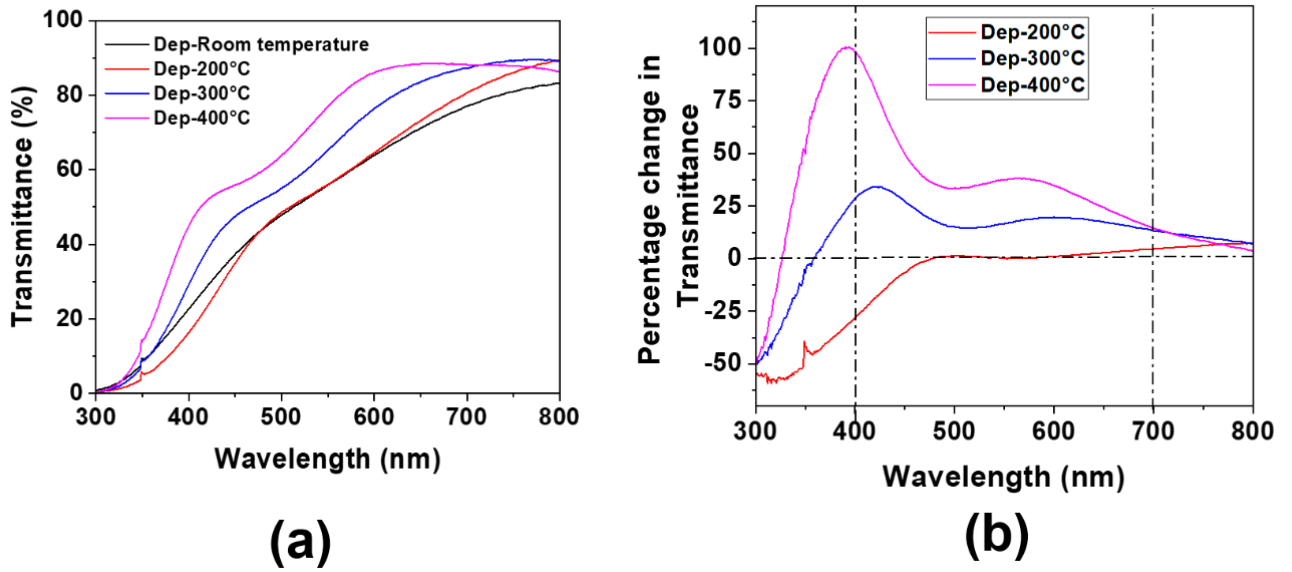


Figure 19: (a): Transmittance spectra of CuInO_x films on quartz at different temperatures during deposition. (b) Percentage increase in transmittance for the deposited films due to the effect of substrate heating with respect to room temperature deposition

Table 5 The extrapolated values of the bandgap for various substrate temperature

Substrate Temperature (°C)	Bandgap (eV)
Room Temperature	2.46 eV
200°C	2.52 eV
300°C	2.73 eV
400°C	2.99 eV

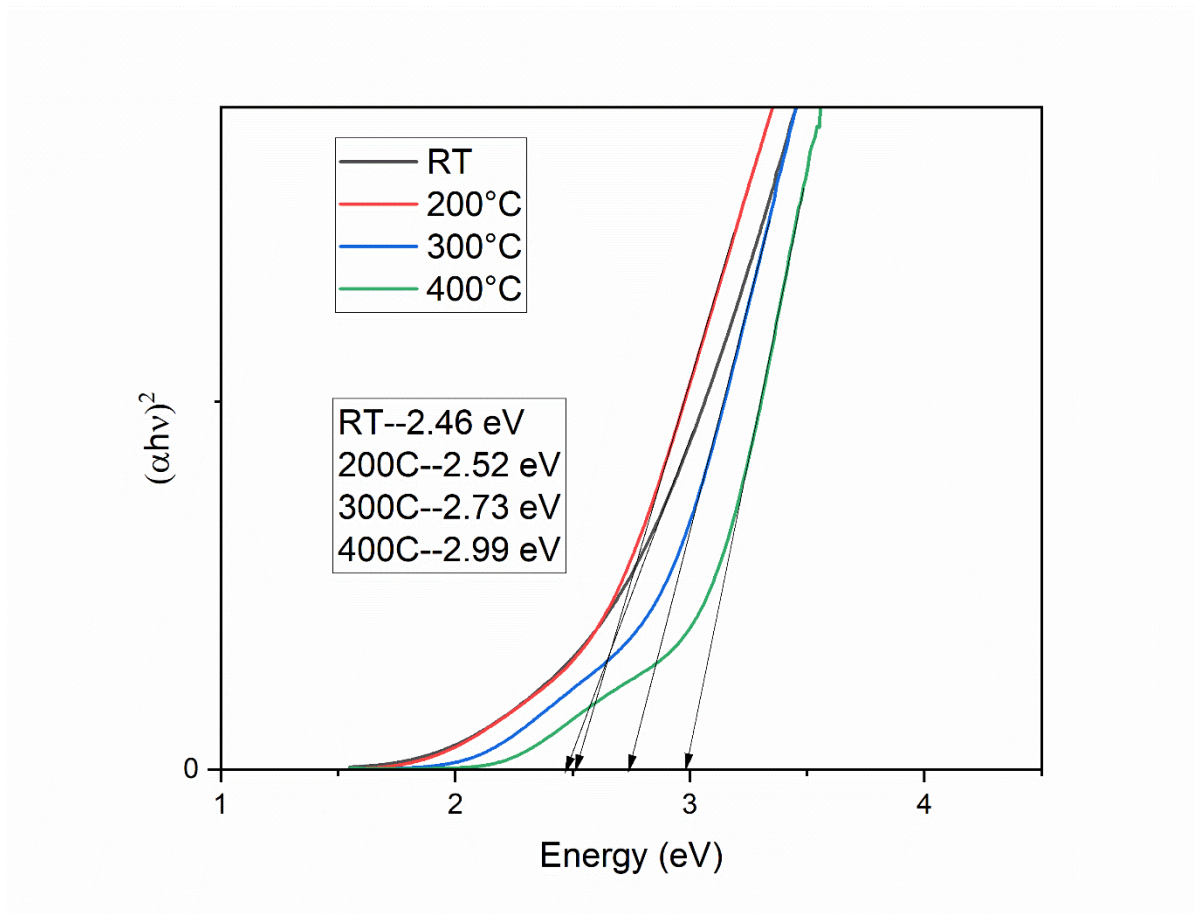


Figure 20: Tauc plots of the CuInO_x thin films deposited at different substrate temperatures

4.2.3 Morphological studies

Figure 21 shows the SEM images of as-deposited CIO thin films as well as those obtained at substrate temperatures of 200°C, 300°C, and 400°C. Changes in the morphology were identified as the substrate heating temperature was increased. Films with a substrate deposition temperature of 200°C displayed the presence of very small grains, as shown in Figure 21 (b) with respect to the film deposited at room temperature. Thus, a minimum of 200°C is required to initiate nanocrystalline growth as evidenced in the figure. However, an increase in the grain size was seen for the films realized at an elevated temperature of 300°C,

which continued to grow at temperatures of 400°C. The grain size of 10-30 nm was obtained for the films deposited at 400°C.

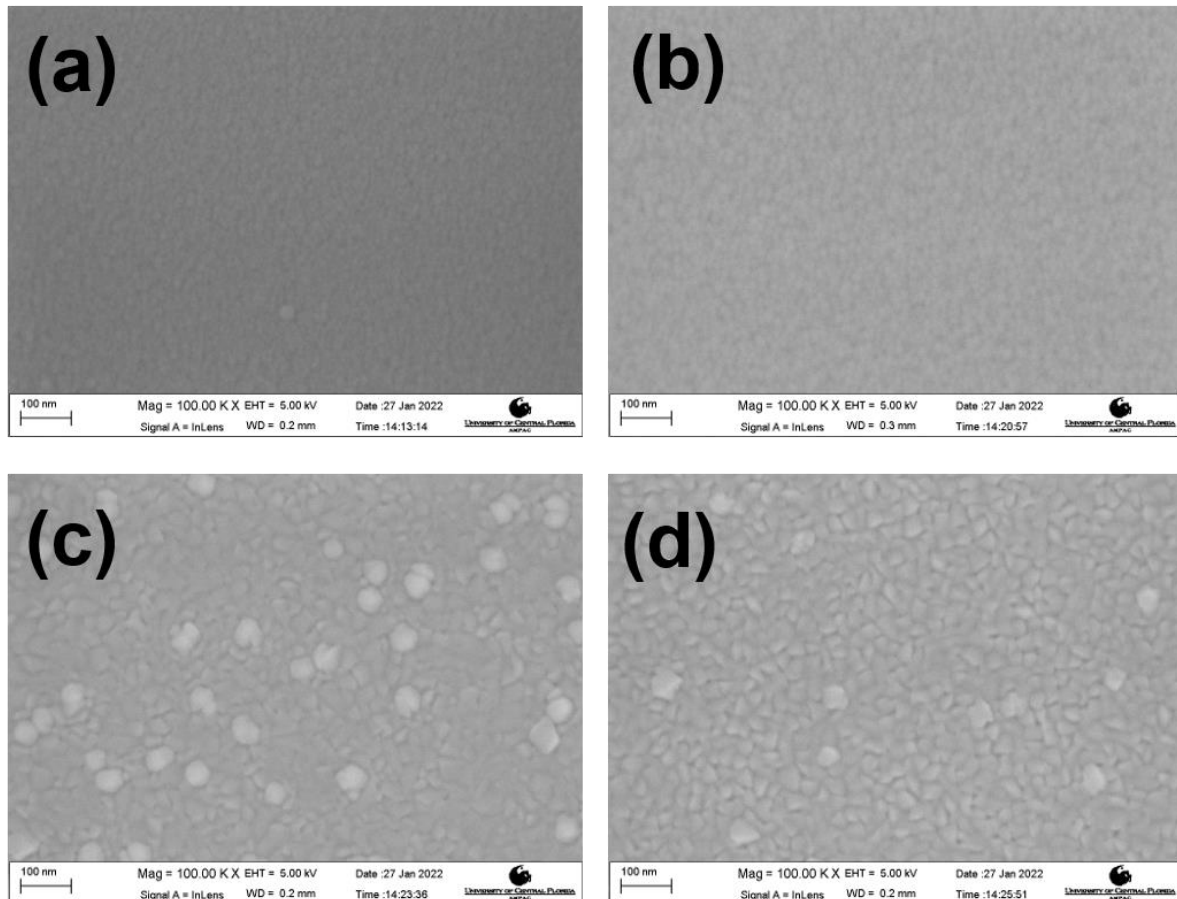


Figure 21: (a): SEM images of CuInO_x films on quartz: (a) room temperature, (b) substrate heater temperature of 200°C, (c) substrate heater temperature of 300°C, (d) substrate heater temperature of 400°C

4.3 Heterojunction Studies

The heterojunction behavior of this material was investigated by fabricating p-n junction using copper indium oxide thin films as the p-type TCO and Indium Tin Oxide as the n-type TCO. The process flow and the characteristics are as follows.

4.3.1 n-Si/p-CIO heterojunction devices

The structures of the fabricated devices as outlined in figure 13 (a). A 1-20 Ω -cm n-type silicon was used to make n-Si/p-CIO heterojunctions. As a back contact for the n-Si, the thermal evaporation technique was used to deposit aluminum in the back of the silicon. The sample was annealed at 400°C for 30 minutes in an N₂ ambiance. An approximately 4000 Å of copper indium oxide was deposited using RF magnetron sputtering at the substrate temperature of 400°C. A mask was used to deposit circular aluminum dots as a contact for the p-Type CIO film. Figure 22 shows the fabricated n-Si/p-CIO heterojunction.

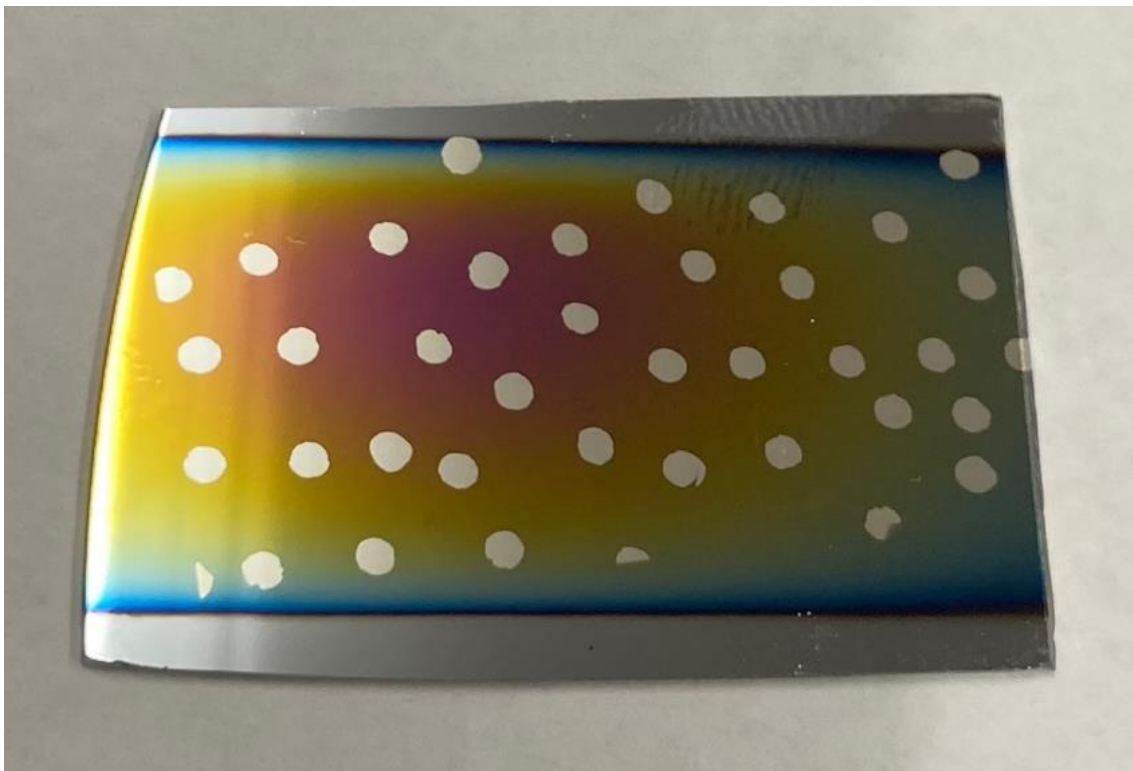


Figure 22: Fabricated n-Si/p-CIO p-n junction devices

The I-V characteristics were performed using Keithly 2450 source meter. For the silicon-based device, a knee voltage of 0.85 V was obtained. The I-V characteristics in the log scale are

depicted in figure 23 which shows n-Si/p-CIO heterojunction behavior as well as the reverse leakage current.

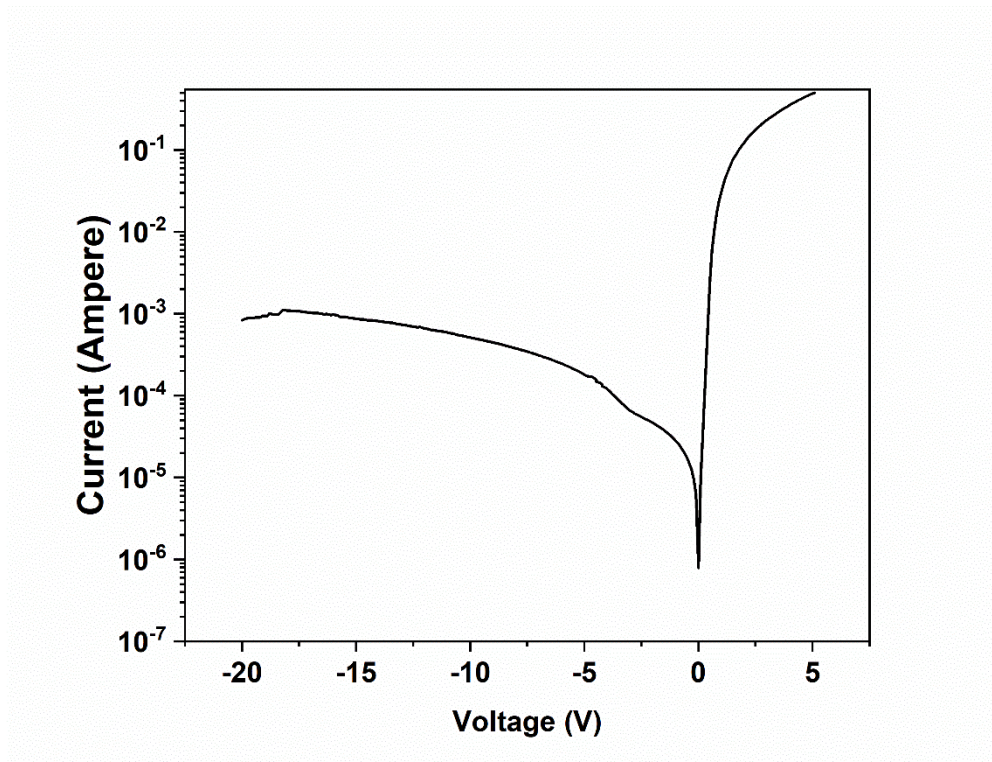


Figure 23: I-V characteristics (butterfly) of n-Si/p-CIO heterojunction devices

Figure 24 shows the I-V forward characteristics of the n-Si/p-CIO heterojunction devices which shows the knee voltage of 0.85 V.

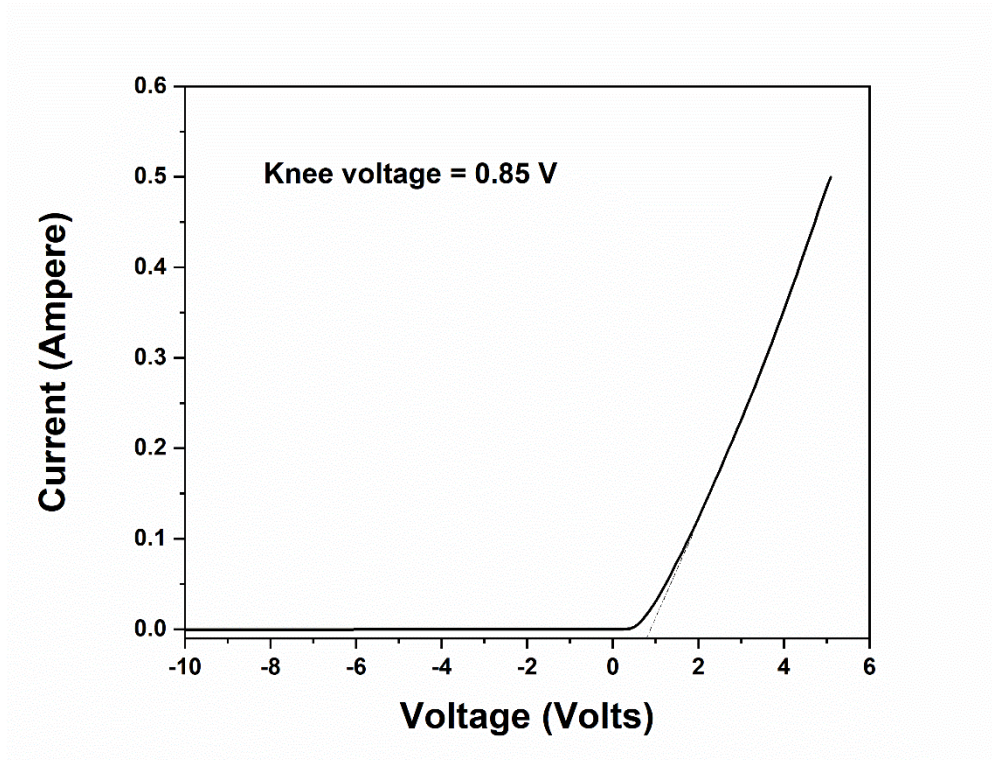


Figure 24: I-V characteristics (forward) of n-Si/p-CIO heterojunction devices

4.3.2 p-CIO/n-ITO heterojunction devices

A quartz substrate was used to fabricate the n-ITO/p-CIO heterojunction on a transparent platform. The structure of the fabricated device as shown in figure 13 (b). CuInOx (p-type) thin films were deposited with a substrate temperature of 400°C. 1 cm x 1 cm area was opened and the rest of the area was masked using aluminum foil. Indium tin oxide (n-type) was deposited by RF magnetron sputtering (100 W, 10 mTorr, 10 sccm Ar) at room temperature to obtain a thickness of ~4000 Å. A mask with several holes (1 mm diameter) is used to deposit aluminum contacts on copper indium oxide (p-type) as well as indium tin oxide (n-type). Figure 25 shows the fabricated p-CIO/n-ITO heterojunction devices on a quartz substrate.



Figure 25: Fabricated p-CIO/n-ITO heterojunction devices

Figure 26 shows the I-V characteristics (butterfly) for the quartz-based p-CIO/n-ITO heterojunction with a knee voltage of 1.6V.

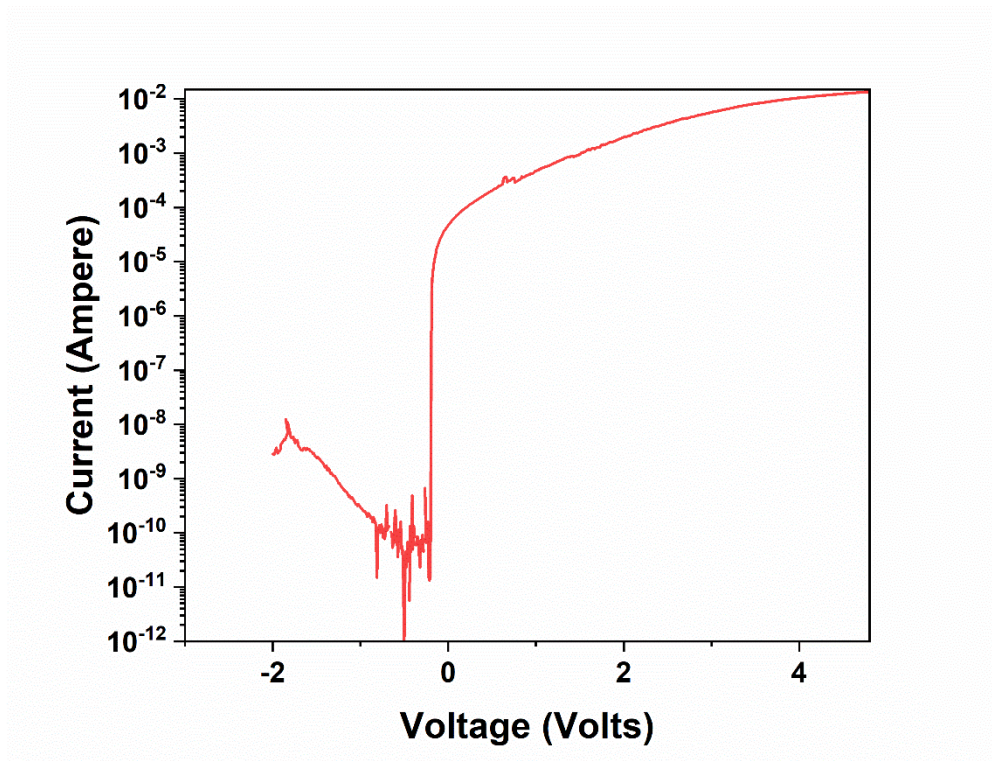


Figure 26: I-V characteristics (butterfly) of p-CIO/n-ITO heterojunction devices

The IV characteristics again confirm a p-CIO/n-ITO heterojunction which has many potential applications in transparent electronics as both the layers have very high transmittance. Figure 25 shows the photomicrograph of the fabricated device on quartz substrate showing high transparency.

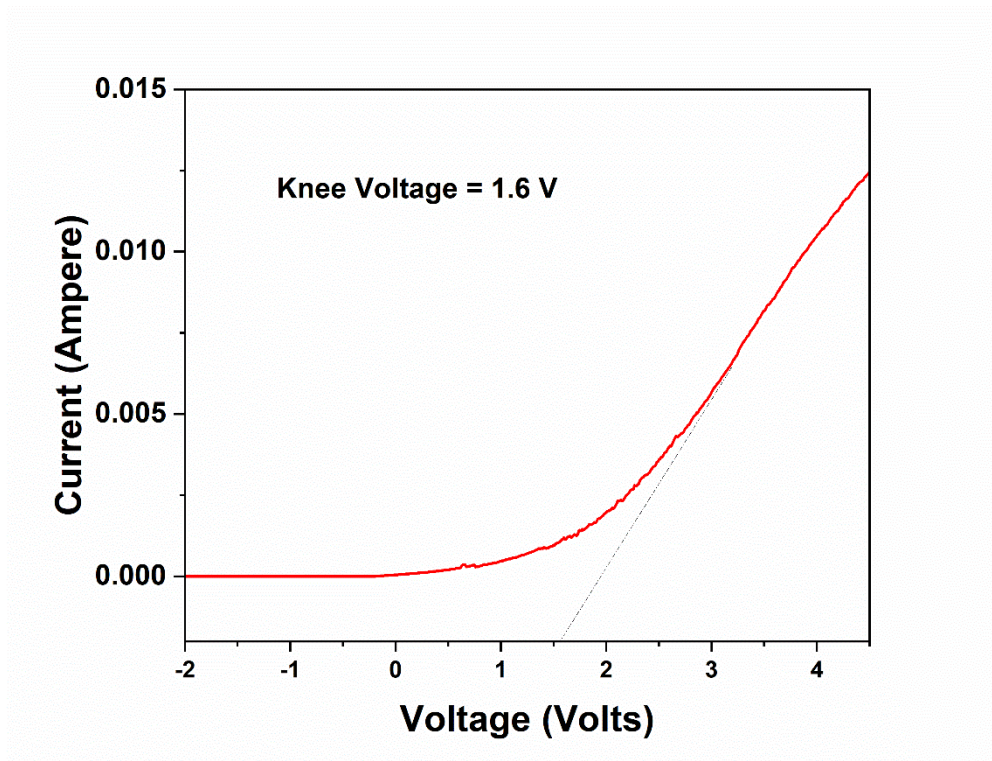


Figure 27: I-V characteristics (forward) of p-CIO/n-ITO heterojunction devices

Figure 27 shows the forward characteristics of the p-CIO/n-ITO heterojunction devices. A knee voltage of 1.6 V was observed in this study. The knee voltage is higher than the silicon-based heterojunction. This is attributed to the bandgap of the devices such as the transparent device has more indium phases which push the bandgap to the higher side since the indium oxide band gap is higher than the silicon.

4.3.3 Heterojunction for light characteristic studies

A 1-20 Ω -cm n-type silicon was used to make n-Si/p-CIO heterojunction for light characteristic study. As a back contact for the n-Si, the thermal evaporation technique was used to deposit aluminum in the back of the silicon. The sample was annealed at 400 °C for 30 minutes in an N₂ ambiance. An approximately 4000 Å of copper indium oxide was deposited using RF magnetron sputtering at the substrate temperature of 400°C. Aluminum foil was used

to wrap the sample and cut the E shape to open the contact for the copper indium oxide film. Aluminum was deposited using the evaporation technique for the contact of the p-Type CIO film. Figure 28 shows the fabricated n-Si/p-CIO heterojunction for the study of the light characteristics.

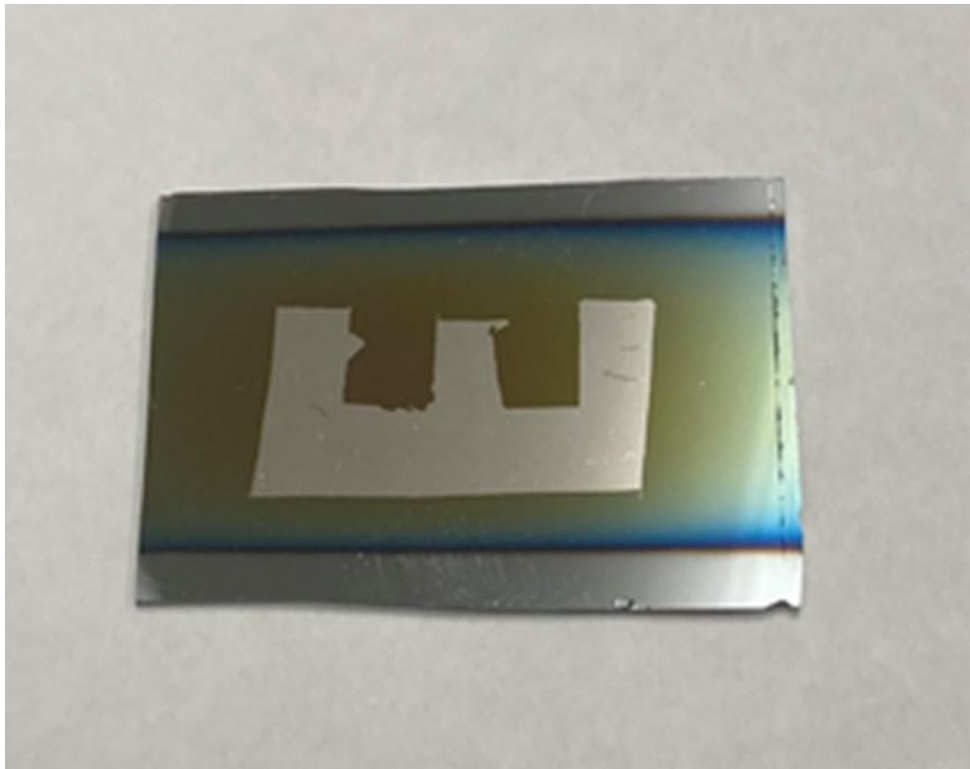


Figure 28: Al/n-Silicon/CI/Al heterojunction for light characteristics performance

Light characteristics were also performed on the device, and an open-circuit voltage of 50 mV and short circuit current of 5 μ A was obtained. This confirms that the device is suitable for optoelectronic applications including solar cells and photodetectors. Figure 29 shows the light characteristics of the fabricated heterojunction.

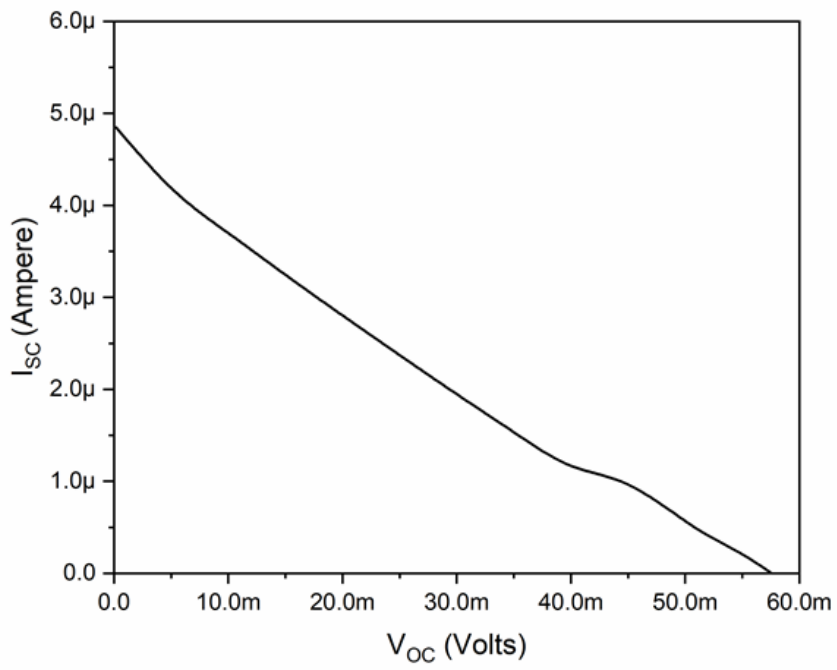


Figure 29: Light characteristics

CHAPTER FIVE: CONCLUSION

The $\text{Cu}_2\text{In}_2\text{O}_5$ thin films were deposited by the RF magnetron sputtering technique. The effects of structural, morphological, optical, and electrical properties due to post-deposition annealing at 100-900°C in constant O_2 flow were studied. Both the XRD analysis and the FESEM images concluded that the minimum annealing temperature of 500°C was required to initiate the crystallization and grain growth. Further increase in annealing temperature increased crystallization and grain size. In addition to $\text{Cu}_2\text{In}_2\text{O}_5$ phases, the XRD results revealed the presence of an additional phase corresponding to In_2O_3 or CuInO_2 . Optical studies showed a bandgap of 3.4-3.6eV for the films. Copper Indium Oxide (CuInO_x) films having a p-type behavior along with high transparency, and superior electrical conductivity was deposited by RF magnetron sputtering. This control over the electrical, morphological, and optical properties was obtained in situ by varying the substrate temperature during the deposition process. While the p-type nature was controlled by the presence of the copper oxide phases in the deposited thin films, the transparency was controlled by the presence of indium oxide phases. XPS results confirm that at elevated temperatures, the addition of indium oxide phases is favored resulting in a higher optical bandgap (2.6-2.99 eV) and better transparency (>60% for 400-700 nm). Optimal optical, electrical, and morphological properties were obtained for depositions carried out at a substrate temperature of 400°C. Heterojunction behavior of the p-type CIO was confirmed with n-Si and n-ITO thereby laying the basis for completely transparent TCO-based optoelectronic devices.

Future Works

Further processes have to be tailored to achieve the delafossite structure of copper indium oxide (CuInO_2). This can be achieved by using various compositions of $\text{Cu}_2\text{O}:\text{In}_2\text{O}_3$ targets. Oxygen can be introduced along with argon in different ratios during sputtering. The other approach is to use the dual sputtering technique with targets of copper and indium oxide in the O_2 ambiance to achieve delafossite structure.

REFERENCES

1. Ginley, D.S. and C. Bright, *Transparent conducting oxides*. MRS bulletin, 2000. **25**(8): p. 15-18.
2. Fortunato, E., et al., *Transparent conducting oxides for photovoltaics*. MRS bulletin, 2007. **32**(3): p. 242-247.
3. Ye, F., et al. *Transparent Conductive Cu-In-O Thin Films Deposited by Reactive DC Magnetron Sputtering with Different Targets*. in *Advanced Materials Research*. 2011. Trans Tech Publ.
4. Chopra, K.L., S. Major, and D.K. Pandya, *Transparent Conductors - a Status Review*. Thin Solid Films, 1983. **102**(1): p. 1-46.
5. Dawar, A.L. and J.C. Joshi, *Semiconducting Transparent Thin-Films - Their Properties and Applications*. Journal of Materials Science, 1984. **19**(1): p. 1-23.
6. Gordon, R.G., *Criteria for choosing transparent conductors*. Mrs Bulletin, 2000. **25**(8): p. 52-57.
7. Saikumar, A.K., G. Skaria, and K.B. Sundaram, *ZnO gate based MOSFETs for sensor applications*. ECS Transactions, 2014. **61**(26): p. 65.
8. Szyszka, B., et al., *Development of new transparent conductors and device applications utilizing a multidisciplinary approach*. Thin Solid Films, 2010. **518**(11): p. 3109-3114.
9. Zhang, B., et al., *Performance of InSnZrO as transparent conductive oxides*. Physica Status Solidi a-Applications and Materials Science, 2010. **207**(4): p. 955-962.
10. Khan, A. and F. Rahman. *Study of microstructural and optical properties of nanocrystalline indium oxide: A transparent conducting oxide (TCO)*. in *AIP Conference Proceedings*. 2019. AIP Publishing LLC.
11. Nehate, S.D., et al., *Work Function Extraction of Indium Tin Oxide Films from MOSFET Devices*. Ecs Journal of Solid State Science and Technology, 2018. **7**(3): p. P87-P90.
12. Sundaram, K.B. and A. Khan, *Characterization and optimization of zinc oxide films by rf magnetron sputtering*. Thin Solid Films, 1997. **295**(1-2): p. 87-91.
13. Shantheyanda, B.P., et al., *Compositional study of vacuum annealed Al doped ZnO thin films obtained by RF magnetron sputtering*. Journal of Vacuum Science & Technology A, 2011. **29**(5): p. 051514.
14. Sundaram, K. and G. Bhagavat, *Chemical vapour deposition of tin oxide films and their electrical properties*. Journal of Physics D: Applied Physics, 1981. **14**(2): p. 333.
15. Banerjee, A. and K. Chattopadhyay, *Recent developments in the emerging field of crystalline p-type transparent conducting oxide thin films*. Progress in Crystal Growth and Characterization of materials, 2005. **50**(1-3): p. 52-105.
16. Su, C.-Y., et al., *Synthesis of Cu₂In₂O₅ and CuInGaO₄ nanoparticles*. Thin solid films, 2013. **531**: p. 42-48.
17. Sundaram, K.B. and A. Khan, *Work function determination of zinc oxide films*. Journal of Vacuum Science & Technology a-Vacuum Surfaces and Films, 1997. **15**(2): p. 428-430.
18. Sundaresh, S., S.D. Nehate, and K.B. Sundaram, *Electrical and Optical Studies of Reactively Sputtered Indium Oxide Thin Films*. Ecs Journal of Solid State Science and Technology, 2021. **10**(6).

19. Noh, J.H., et al., *Indium Oxide Thin-Film Transistors Fabricated by RF Sputtering at Room Temperature*. Ieee Electron Device Letters, 2010. **31**(6): p. 567-569.
20. Kawazoe, H., et al., *P-type electrical conduction in transparent thin films of CuAlO₂*. Nature, 1997. **389**(6654): p. 939-942.
21. Biswas, S.K., et al., *Studies on the sensing behaviour of nanocrystalline CuGa₂O₄ towards hydrogen, liquefied petroleum gas and ammonia*. Talanta, 2010. **81**(4-5): p. 1607-1612.
22. Fenner, L., et al. *Zero-point entropy of the spinel spin glasses CuGa₂O₄ and CuAl₂O₄*. in *Journal of Physics: Conference Series*. 2009. IOP Publishing.
23. Makhova, L., et al., *X - ray spectroscopic investigation of forbidden direct transitions in CuGaO₂ and CuInO₂*. physica status solidi (a), 2006. **203**(11): p. 2861-2866.
24. Pilliadugula, R., C. Nithya, and N.G.J.N.A. Krishnan, *Influence of Ga₂O₃, CuGa₂O₄ and Cu₄O₃ phases on the sodium-ion storage behaviour of CuO and its gallium composites*. Nanoscale Adv, 2020. **2**(3): p. 1269-1281.
25. Saikumar, A.K., et al., *Properties of RF Magnetron-Sputtered Copper Gallium Oxide (CuGa₂O₄) Thin Films*. Coatings, 2021. **11**(8): p. 921.
26. Shi, J., et al., *Preparation of high-quality CuGa₂O₄ film via annealing process of Cu/β-Ga₂O₃*. J. Mater. Sci. , 2019. **54**(16): p. 11111-11116.
27. Su, C.Y., et al., *Synthesis of Cu₂In₂O₅ and CuInGaO₄ nanoparticles*. Thin Solid Films, 2013. **531**: p. 42-48.
28. Su, C.-Y., et al., *Effects of Cu₂S sintering aid on the formation of CuInS₂ coatings from single crystal Cu₂In₂O₅ nanoparticles*. Surface and Coatings Technology, 2013. **231**: p. 517-520.
29. Wang, J., et al., *Solution Synthesized p-Type Copper Gallium Oxide Nanoplates as Hole Transport Layer for Organic Photovoltaic Devices*. Journal of Physical Chemistry Letters, 2015. **6**(6): p. 1071-1075.
30. Wei, H.L., et al., *Epitaxial growth and characterization of CuGa₂O₄ films by laser molecular beam epitaxy*. Aip Advances, 2017. **7**(11): p. 115216.
31. Yin, H., et al., *Synthesis of spinel-type CuGa₂O₄ nanoparticles as a sensitive non-enzymatic electrochemical sensor for hydrogen peroxide and glucose detection*. Journal of Electroanalytical Chemistry, 2021. **885**: p. 115100.
32. Zardkhoshoui, A.M. and S.S.H. Davarani, *Designing a flexible all-solid-state supercapacitor based on CuGa₂O₄ and FeP-rGO electrodes*. Journal of Alloys and Compounds, 2019. **773**: p. 527-536.
33. Singh, M., V. Singh, and B. Mehta, *Synthesis and properties of nanocrystalline copper indium oxide thin films deposited by RF magnetron sputtering*. Journal of Nanoscience and Nanotechnology, 2008. **8**(8): p. 3889-3894.
34. Nair, B.G., et al., *Calcium incorporated copper indium oxide thin films-a promising candidate for transparent electronic applications*. Thin Solid Films, 2020. **693**: p. 137673.
35. Saikumar, A.K., S.D. Nehate, and K.B. Sundaram, *Review-RF Sputtered Films of Ga₂O₃*. Ecs Journal of Solid State Science and Technology, 2019. **8**(7): p. Q3064-Q3078.
36. Marquardt, M.A., N.A. Ashmore, and D.P. Cann, *Crystal chemistry and electrical properties of the delafossite structure*. Thin Solid Films, 2006. **496**(1): p. 146-156.
37. Mackenzie, A.P., *The properties of ultrapure delafossite metals*. Reports on Progress in Physics, 2017. **80**(3): p. 032501.

38. Nagarajan, R., et al., *p-Type conductivity in the delafossite structure*. International Journal of Inorganic Materials, 2001. **3**(3): p. 265-270.
39. Sasaki, M. and M. Shimode, *Fabrication of bipolar CuInO₂ with delafossite structure*. Journal of Physics and Chemistry of Solids, 2003. **64**(9-10): p. 1675-1679.
40. Yanagi, H., et al., *Fabrication of all oxide transparent p-n homojunction using bipolar CuInO₂ semiconducting oxide with delafossite structure*. Solid state communications, 2001. **121**(1): p. 15-17.
41. Qiu, Z., et al., *Enhanced physical properties of pulsed laser deposited NiO films via annealing and lithium doping for improving perovskite solar cell efficiency*. Journal of Materials Chemistry C, 2017. **5**(28): p. 7084-7094.
42. Wang, T., et al., *Low temperature synthesis wide optical band gap Al and (Al, Na) co-doped ZnO thin films*. Applied Surface Science, 2011. **257**(6): p. 2341-2345.
43. Arca, E., K. Fleischer, and I. Shvets, *Magnesium, nitrogen codoped Cr₂O₃: A p-type transparent conducting oxide*. Applied Physics Letters, 2011. **99**(11): p. 111910.
44. Götzendörfer, S. and P. Löbmann, *Influence of single layer thickness on the performance of undoped and Mg-doped CuCrO₂ thin films by sol-gel processing*. Journal of sol-gel science and technology, 2011. **57**(2): p. 157-163.
45. Lau, C.H., L. Zhuang, and K. Wong, *In - doped transparent and conducting cubic magnesium zinc oxide thin films grown by pulsed laser deposition*. physica status solidi (b), 2007. **244**(5): p. 1533-1537.
46. Ellmer, K. and G. Vollweiler, *Electrical transport parameters of heavily-doped zinc oxide and zinc magnesium oxide single and multilayer films heteroepitaxially grown on oxide single crystals*. Thin Solid Films, 2006. **496**(1): p. 104-111.
47. Ingram, B.J., et al., *Point defects and transport mechanisms in transparent conducting oxides of intermediate conductivity*. Thin Solid Films, 2005. **486**(1-2): p. 86-93.
48. Nair, B.G., et al., *Tin-incorporated nanostructured copper indium oxide delafossite thin films: Structural, electrical and optical analysis*. Journal of Alloys and Compounds, 2018. **746**: p. 435-444.
49. Su, C.Y., et al., *Effects of Cu₂S sintering aid on the formation of CuInS₂ coatings from single crystal Cu₂In₂O₅ nanoparticles*. Surface & Coatings Technology, 2013. **231**: p. 517-520.
50. Skaria, G., et al., *Annealing Studies of Copper Indium Oxide (Cu₂In₂O₅) Thin Films Prepared by RF Magnetron Sputtering*. Coatings, 2021. **11**(11): p. 1290.
51. Ohyama, M., H. Kozuka, and T. Yoko, *Sol - gel preparation of transparent and conductive aluminum - doped zinc oxide films with highly preferential crystal orientation*. Journal of the American Ceramic Society, 1998. **81**(6): p. 1622-1632.
52. Sundaram, K. and G. Bhagavat, *Optical absorption studies on tin oxide films*. Journal of Physics D: Applied Physics, 1981. **14**(5): p. 921.